

Quantum Resonances in a Complex-Momentum Basis

Bachelor Thesis in Physics

Jonathan Bengtsson, Ola Embréus, Vincent Ericsson,
Pontus Granström, Nils Wireklint

Department of Fundamental Physics
CHALMERS UNIVERSITY OF TECHNOLOGY
Göteborg, Sverige 2013
FUFX02-13-03

Abstract

Resonances are important features of open quantum systems. We study, in particular, unbound and loosely bound nuclear systems. We model ${}^5\text{He}$ and ${}^6\text{He}$ in a few-body picture, consisting of an alpha-particle core with one and two valence neutrons respectively. Basis-expansion theory is briefly explained and then used to expand the nuclear system in the harmonic oscillator and momentum bases. We extend the momentum basis into the complex plane, obtaining the so-called Berggren basis. With the complex-momentum method we are able to reproduce the observed resonances in ${}^5\text{He}$. The ${}^5\text{He}$ Berggren basis solutions are used as a single-particle basis to create many-body states in which we expand the ${}^6\text{He}$ system. For the two-body interaction between the neutrons, we use two different phenomenological models: a Gaussian and a Surface Delta Interaction (SDI). The strength of each interaction is fitted to reproduce the ${}^6\text{He}$ ground state energy. With the Gaussian interaction we do not obtain the ${}^6\text{He}$ resonance, whereas with the SDI we do. The relevant parts of the second quantization formalism is summarized, and we provide details for its implementation.

Contents

1	Introduction	1
2	The Basis Expansion Method	5
2.1	Spherical Symmetry	6
2.2	The Harmonic Oscillator Basis	7
2.3	The Momentum Basis	8
2.3.1	Discretization and Symmetrization	9
2.4	Numerical Considerations	10
3	The Two-Body Nuclear System	11
3.1	The Nuclear Shell Model	11
3.1.1	The Woods-Saxon Potential	12
3.1.2	Magic Nuclei	12
3.2	The ${}^5\text{He}$ Nucleus	13
3.2.1	Harmonic Oscillator Basis	14
3.2.2	Momentum Basis	15
4	The Complex-Momentum Basis	18
4.1	The Complex Momentum Plane	18
4.1.1	The Berggren Completeness Relation	19
4.2	${}^5\text{He}$ Revisited	20
4.2.1	The Discretized Complex Contour	20
4.2.2	The ${}^5\text{He}$ Resonances	21
4.2.3	Fitting to Experimental Resonance Data	25
5	Many-Body Theory and Implementation	26
5.1	Identical Particles	26
5.1.1	Antisymmetric Fermion states	27
5.2	Second quantization	28
5.2.1	Creation and Annihilation Operators	28
5.2.2	General Operators in Fock Space	29

5.3	Angular Momentum Coupling	31
5.3.1	The Two-Particle Coupled Basis	31
5.3.2	Antisymmetrizing the Coupled Basis	32
5.3.3	Coupled Matrix Elements	33
5.4	Second Quantization Implementation	34
5.4.1	Single-Particle-State Objects	34
5.4.2	Fock State Objects and Operator Functions	34
5.4.3	Fock Operator Matrix Elements	35
6	The Nuclear Three-Body Problem	36
6.1	The ${}^6\text{He}$ Nucleus	37
6.2	Neutron-Neutron Interaction	37
6.2.1	Gaussian Interaction	38
6.2.2	Surface Delta Interaction	39
6.3	The ${}^6\text{He}$ Solutions	40
6.3.1	Identifying the Resonance	40
6.3.2	Using the Gaussian Interaction	40
6.3.3	Using the Surface Delta Interaction	41
6.3.4	${}^6\text{He}$ in the Real Momentum Basis	41
7	Outlook	43
7.1	Realistic Two-Body Interactions	43
7.2	Additional Nucleons and Other Elements	44
7.3	Reducing Computation Time	44
A	Derivations	48
A.1	Harmonic Oscillator Matrix Elements	48
A.2	Radial Momentum Space TISE	49
B	Numerical Integration	51
B.1	Gauss-Legendre Quadrature	51
C	Tools	52

Chapter 1

Introduction

The properties of a quantum mechanical system are determined by its Hamiltonian. Particles in a potential well with infinitely high walls form localized bound states. Such a system is called a *closed quantum system*, since the number of particles is conserved and the particles are localized in a finite region. The energy of a closed quantum system can only take on discrete values, as illustrated in Fig. 1.1a with the harmonic oscillator potential.

An *open quantum system*, on the other hand, portrayed in Fig. 1.1c, is a system with a finite potential. For a system with a vanishing potential particles can enter and exit the system and, consequently, there are unbound states. For a trivial potential these are just free particle states but for a non-negligible potential these are denoted *scattering states*. Depending on the depth of the potential well of the open system, there can be a finite number of bound states.

In addition to the bound and unbound states, some open quantum systems harbor *resonances*. These are *quasi-bound* states that are neither bound nor unbound, but exhibit properties of both.

They appear in the continuum, like unbound states, but are localized, like bound states. However, the wavefunction of a resonance is only localized for a finite amount of time, as opposed to a bound, *stationary* state that forever stays the same. A resonance can be described with a complex energy, as the following argument suggests.

The state of a particle is described by its wavefunction ψ , which can be written as the product of a function of time and position

$$\psi(t, \mathbf{r}) = \psi_t(t)\psi_r(\mathbf{r}). \quad (1.1)$$

The wavefunction evolves according to the Time-Dependent Schrödinger Equation (TDSE)

$$i\hbar \frac{\partial}{\partial t} |\psi\rangle = H|\psi\rangle. \quad (1.2)$$

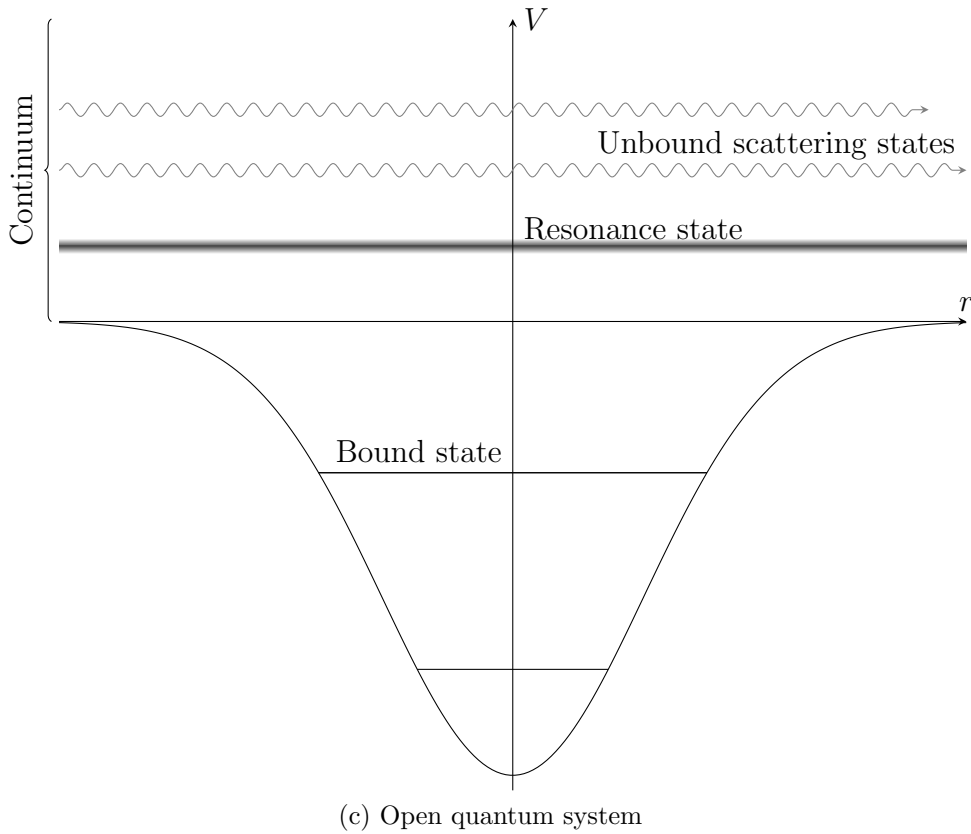
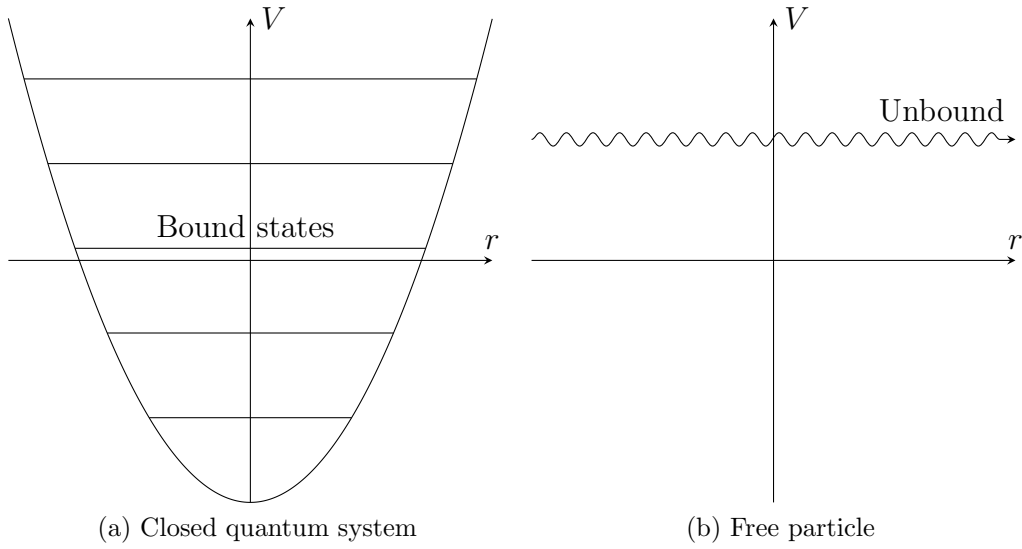


Figure 1.1: Three different quantum systems: the closed harmonic oscillator, the free particle and an open gaussian well.

An eigenstate of the Hamiltonian H with energy E , i.e. a solution to the Time-Independent Schrödinger Equation (TISE)

$$H|\psi\rangle = E|\psi\rangle \quad (1.3)$$

has the simple time evolution

$$\psi(t, \mathbf{r}) = \exp\left(-\frac{iE}{\hbar}t\right)\psi_t(0)\psi_{\mathbf{r}}(\mathbf{r}). \quad (1.4)$$

With the energy E real, the exponential factor is just a phase and the probability $|\psi(t, \mathbf{r})|^2$ of finding the particle at a given \mathbf{r} is unchanged over time. However, if we let the energy be complex

$$E = E_0 - i\frac{\Gamma}{2}, \quad (1.5)$$

we get

$$|\psi(t, \mathbf{r})|^2 = \left| \exp\left(-\frac{iE_0}{\hbar}t\right) \exp\left(-\frac{\Gamma}{2\hbar}t\right) \psi(0, \mathbf{r}) \right|^2 = \exp\left(-\frac{\Gamma}{\hbar}t\right) |\psi(0, \mathbf{r})|^2 \quad (1.6)$$

describing a resonance state decaying exponentially with half-life $t_{1/2} = \hbar \ln 2 / \Gamma$. This parameter Γ is called the *width* of the resonance.

We want to use the simpler formalism of the TISE, as opposed to the more general TDSE, and we see that this is possible by letting the resonance have a complex energy. However, complex eigenvalues pose a problem in standard quantum mechanics, where operators are postulated to be Hermitian. Hermitian operators can only have real eigenvalues, and are thus insufficient for treating resonances.

The aim of this thesis is to present methods for describing resonances using the TISE in a complex-energy framework. To demonstrate the methods, we will study the simple nuclear systems ${}^5\text{He}$ and ${}^6\text{He}$. They are relevant because the ground state of ${}^5\text{He}$ and the first excited state of both ${}^5\text{He}$ and ${}^6\text{He}$ are resonances. Despite the unbound nature of ${}^5\text{He}$, the ground state of ${}^6\text{He}$ is actually bound, an example of a *Borromean* system, named after the Borromean rings depicted on the cover of this thesis.

The thesis can conceptually be divided into two parts, the first covering resonances in a simple two-body problem and the second part covering the first steps toward more complicated many-body systems. In Chapter 2 the *basis expansion* method for solving the Schrödinger equation is introduced. The basis expansion method is then used in Chapter 3 to study a loosely bound two-body nuclear system, the ${}^5\text{He}$ nucleus. In Chapter 4 we use the Berggren basis to reproduce the resonance in ${}^5\text{He}$.

Chapter 5 is an introduction to many-body theory, focusing on fermionic systems. The many-body theory is then utilized in Chapter 6 to study a three-body problem, specifically the ${}^6\text{He}$ nucleus. Finally, Chapter 7 is an outlook discussing further development of the methods.

Chapter 2

The Basis Expansion Method

We want to study loosely bound quantum systems by solving the *Time Independent Schrödinger Equation* (TISE)

$$H|\psi\rangle = E|\psi\rangle, \quad (2.1)$$

commonly written in the position basis as

$$\left(-\frac{\hbar^2}{2m}\nabla^2 + V(\mathbf{r})\right)\psi(\mathbf{r}) = E\psi(\mathbf{r}). \quad (2.2)$$

For the nuclear systems to be treated, the TISE has no known analytical solutions, and we need to use numerical methods to solve it. We will use the basis expansion method, writing the equation as an eigenvalue problem

$$\sum_j H_{ij}\psi_j = E\psi_i \quad (2.3)$$

with a finite matrix H that we can diagonalize to find the eigenvalues E .

To write the TISE as a matrix equation we use *basis expansion*. Basis expansion is how we make sense of the abstract Hilbert spaces, operators and state vectors of Quantum Mechanics (QM). By expanding these abstract objects in a basis, we can relate them to the physical world. For example, (2.2) is the TISE for a single particle, expanded in the position basis. We will not expand our problems in the position basis, but it will still be important, since it is the most natural basis to express the potential in.

Before we begin, we briefly recap some well known QM facts. First we need a *complete basis*, either discrete, $|n\rangle$, or continuous, $|x\rangle$. A complete basis means that any state $|\psi\rangle$ can be written as a linear combination of the basis states

$$|\psi\rangle = \sum_n \psi_n |n\rangle \quad \text{or} \quad |\psi\rangle = \int dx \psi(x) |x\rangle. \quad (2.4)$$

The complete bases we will use in this thesis are the *position basis* $|\mathbf{r}\rangle$, the *momentum basis* $|\mathbf{k}\rangle$, the *harmonic oscillator basis* $|nlm\rangle$ and the elusive *Berggren basis* [1]. All these bases are orthonormal, i.e. all the basis vectors satisfy

$$\langle n|n'\rangle = \delta_{nn'} \quad \text{or} \quad \langle x|x'\rangle = \delta(x - x') \quad (2.5)$$

depending on if the base is discrete or continuous. With a complete basis $|n\rangle$, we get the very useful *completeness relation*

$$I = \sum_n |n\rangle\langle n| \quad \text{or} \quad I = \int dx |x\rangle\langle x|, \quad (2.6)$$

where I is the identity operator. This relation can thus be inserted anywhere in any equation, and will find frequent use in this thesis.

Let us now expand the TISE in the abstract $|n\rangle$ basis. We start by inserting the completeness relation for $|n\rangle$ in (2.1)

$$H \left(\sum_{n'} |n'\rangle\langle n'| \right) |\psi\rangle = \sum_{n'} H |n'\rangle\langle n'|\psi\rangle = E|\psi\rangle. \quad (2.7)$$

Multiplying (2.4) with $\langle n|$ from the left and using orthonormality, we see that $\langle n'|\psi\rangle = \psi_{n'}$. If we now close (2.7) with $\langle n|$ on the left

$$\sum_{n'} \langle n|H|n'\rangle\psi_{n'} = E\langle n|\psi\rangle, \quad (2.8)$$

and write $H_{nn'} = \langle n|H|n'\rangle$, we get

$$\sum_{n'} H_{nn'}\psi_{n'} = E\psi_n, \quad (2.9)$$

which is equivalent to the matrix equation (2.3). This is the basic method of expanding the TISE in a basis.

2.1 Spherical Symmetry

We limit ourselves to spherically symmetric systems, i.e. systems with a potential $V(r)$ that only depends on the radial distance r . If we considered three-dimensional systems with arbitrary potentials, the matrices would be very large and solving the problem would become infeasible.

Spherical symmetry allows us to write the wavefunction $\psi(\mathbf{r})$ as a product of a radial wavefunction $R(r)$ and a spherical harmonic $Y_l^m(\Omega_r)$

$$\psi(\mathbf{r}) = R_{nl}(r)Y_l^m(\Omega_r). \quad (2.10)$$

$$\begin{pmatrix}
l_1 m_1 & l_1 m_2 & \dots & & \\
\boxed{} & & & & \\
& \boxed{} & & & \\
& & & \ddots & \\
& & & & \dots \\
& & & & & \mathbf{0}
\end{pmatrix}$$

Figure 2.1: An illustration of a block diagonal matrix. The eigenvalues of different blocks are independent of each other. Thus the blocks can be diagonalized separately.

Here l and m are the quantum numbers for the orbital angular momentum and its projection along an arbitrary z -axis. For the matrix elements we find, using the orthonormality of the spherical harmonics,

$$\begin{aligned}
\langle nlm|V|n'l'm'\rangle &= \int_0^\infty dr r^2 \overline{R_{nl}(r)} R_{n'l'}(r) V(r) \int d\Omega_r \overline{Y_l^m(\Omega_r)} Y_{l'}^{m'}(\Omega_r) \\
&= \delta_{mm'} \delta_{ll'} \int_0^\infty dr r^2 \overline{R_{nl}(r)} R_{n'l'}(r) V(r)
\end{aligned} \tag{2.11}$$

meaning that the matrix will be *block diagonal*, illustrated in Fig. 2.1. This means that systems with different l and m can be treated separately. We say that H is *diagonal in l and m* .

2.2 The Harmonic Oscillator Basis

We now expand the TISE in the spherically symmetric Harmonic Oscillator (HO) basis. The basis consists of the eigenstates $|nlm\rangle$ of the HO Hamiltonian

$$H_{\text{HO}} = \frac{p^2}{2\mu} + \frac{\mu\omega^2 r^2}{2}, \tag{2.12}$$

where μ is the mass of the problem and ω is the angular frequency of the oscillator. The expansion procedure is the same as in (2.7) to (2.9) and gives us

$$\sum_{n'l'm'} \langle nlm|H|n'l'm'\rangle \psi_{n'l'm'} = E\psi_{nlm} \tag{2.13}$$

and if we use the fact that H is diagonal in l and m we get

$$\sum_{n'} \langle nlm | H | n'lm \rangle \psi_{n'lm} = E \psi_{nlm}. \quad (2.14)$$

We now have a matrix equation, but we need to find the matrix elements $\langle nlm | H | n'lm \rangle$. These require some calculation (details are in Appendix A.1) and the result is

$$\begin{aligned} \langle nlm | H | n'lm \rangle &= \frac{\hbar\omega}{2} \left(\left(2n + l + \frac{3}{2} \right) \delta_{nn'} + \sqrt{n(n+l+\frac{1}{2})} \delta_{n,n'-1} \right. \\ &\left. + \sqrt{n'(n'+l+\frac{1}{2})} \delta_{n',n-1} \right) + \int_0^\infty dr r^2 R_{nl}(r) V(r) R_{n'l}(r) \end{aligned} \quad (2.15)$$

where R_{nl} are the radial wavefunctions of the harmonic oscillator,

$$R_{nl}(r) = \sqrt{\frac{2 \left(\frac{n-l}{2}\right)!}{\Gamma\left(\frac{n+l}{2} + \frac{3}{2}\right)}} \frac{r^l}{r_0^{l+\frac{3}{2}}} \exp\left(-\frac{r^2}{2r_0^2}\right) L_{(n-l)/2}^{(l+\frac{1}{2})}\left(\frac{r^2}{r_0^2}\right), \quad (2.16)$$

$r_0 = \sqrt{\hbar/\mu\omega}$ is the range and $L_\nu^\lambda(x)$ are the generalized Laguerre polynomials. The radial wavefunction $R(r)$ of a state will be expressed as a linear combination of the harmonic oscillator radial wavefunctions:

$$R(r) = \sum_n \psi_{nl} R_{nl}(r). \quad (2.17)$$

2.3 The Momentum Basis

The momentum, or plane wave, basis has eigenstates $|\mathbf{k}\rangle$, each describing a free particle with momentum \mathbf{p} or wavevector $\mathbf{k} = \mathbf{p}/\hbar$. We will only use \mathbf{k} and refer to it as momentum.

The expansion is done in the same way as before, giving us

$$\int d^3\mathbf{k}' \langle \mathbf{k} | H | \mathbf{k}' \rangle \Phi(\mathbf{k}') = E \Phi(\mathbf{k}), \quad (2.18)$$

where we denote the momentum space wavefunctions with Φ . As in position space, these can be separated into a radial and angular part. This is shown in Appendix A.2 along with the fact that the Schrödinger equation can be written as

$$H\phi(k) = \frac{k^2}{2\mu} \phi(k) + \int_0^\infty dk' k'^2 V(k, k') \phi(k') = E\phi(k) \quad (2.19)$$

$$V(k, k') = \frac{2}{\pi} \int_0^\infty dr r^2 V(r) j_l(kr) j_l(k'r), \quad (2.20)$$

where $\phi(k)$ is the radial part of the momentum space wavefunction and $j_l(kr)$ are the spherical bessel functions of order l . The momentum space radial wavefunction $\phi(k)$ is related to the position space radial wavefunction by

$$R(r) = i^l \sqrt{\frac{2}{\pi}} \int_0^\infty dk k^2 \phi(k) j_l(kr). \quad (2.21)$$

2.3.1 Discretization and Symmetrization

The integral equation (2.19) can be rewritten as a matrix equation through discretization, turning the integral into a sum over a finite set of points k_j and dk into a set of weights w_j :

$$\frac{k_i^2}{2\mu} \phi(k_i) + \sum_{j=1}^N w_j k_j^2 V(k_i, k_j) \phi(k_j) = E \phi(k_i). \quad (2.22)$$

A particular set of points and corresponding weights is called a *quadrature*, and the choice of quadrature greatly impacts the precision of the result. A naïve quadrature with evenly spaced $k_j = j\Delta k$ and a constant weight $w_j = \Delta k$ converges slowly, and should not be used. We instead use the Gauss-Legendre quadrature, for details see Appendix B.1.

With this discretization the Schrödinger equation may be written as

$$\sum_j H_{ij} \phi(k_j) = E \phi(k_i) \quad (2.23)$$

where

$$H_{ij} = \frac{k_i^2}{2\mu} \delta_{ij} + w_j k_j^2 V_{ij} \quad (2.24)$$

$$V_{ij} = \frac{2}{\pi} \int_0^\infty dr r^2 V(r) j_l(k_i r) j_l(k_j r). \quad (2.25)$$

Because of the k_j^2 in the second term of the matrix elements (2.24), the H_{ij} matrix will not be symmetric. Working with a symmetric matrix is faster, which will be explained in the following section. We perform the transformation

$$\begin{aligned} \phi(k_i) &\mapsto \phi'(k_i) = \sqrt{w_i} k_i \phi(k_i) \\ H_{ij} &\mapsto H'_{ij} = \sqrt{\frac{w_i}{w_j}} \frac{k_i}{k_j} H_{ij}, \end{aligned} \quad (2.26)$$

which gives us a symmetric matrix

$$H'_{ij} = \frac{k_i^2}{2\mu} \delta_{ij} + \sqrt{w_i w_j} k_i k_j V_{ij}. \quad (2.27)$$

The Schrödinger equation then becomes

$$\sum_j H'_{ij} \phi'(k_j) = E \phi'(k_j), \quad (2.28)$$

with the same eigenvalues E , meaning that we can work with the symmetric H'_{ij} matrix. Another benefit of the symmetrization is that the norm of the $\phi'(k_i)$ incorporates the weights $w_i k_i^2$. The real space radial wavefunction $R(r)$ is expressed in terms of $\phi'(k_j)$ as

$$R(r) = i^l \sqrt{\frac{2}{\pi}} \sum_{j=1}^N \sqrt{w_j} k_j \phi'_j j_l(k_j r). \quad (2.29)$$

2.4 Numerical Considerations

In order to perform basis expansion on a computer, we need to consider the numerical aspects of the problem. This includes truncation of the basis, matrix size reduction, numerical integration and eigensolver optimizations. The momentum basis is continuous and thus requires special treatment.

The $|nlm\rangle$ and $|k\rangle$ bases are infinite, so we truncate them by only including a finite number N of states in the basis. For an orthonormal basis, the best approximation is to include the N first states. The more states we include in the basis, the more accurate results we get.

The truncation gives us an $N \times N$ Hamiltonian matrix H and the TISE can be written in matrix notation as

$$H\psi = E\psi, \quad (2.30)$$

where the ψ are eigenvectors. We compute the matrix elements H_{ij} with (2.15) and (2.27), carrying out the integrals with the Gauss-Legendre quadrature rule (see Appendix B.1) and setting the upper limit to a finite number. If the matrix is hermitian or symmetric, we only need to consider the elements in the upper triangle including the diagonal, roughly halving the number of computed elements.

When the matrix elements have been computed, the matrix is diagonalized using a standard eigensolver algorithm. For hermitian matrices we use a specialized, faster algorithm.

Chapter 3

The Two-Body Nuclear System

In this chapter we investigate a simple two-body nuclear system using the basis expansion methods from the previous chapter. We begin by discussing the shell model, the Woods-Saxon potential and our model system, ${}^5\text{He}$. The Schrödinger equation is then solved in the HO and momentum bases. The solutions are studied by looking at the energies and wavefunctions while varying parameters.

3.1 The Nuclear Shell Model

A typical example of an open quantum system is the atomic nucleus encountered in nuclear physics. The atomic nucleus is held together by the short-ranged strong interaction acting between all nucleons and is commonly studied within a shell model. This is done by introducing a *mean-field* potential, often by the following procedure [2]:

Consider the Hamiltonian for a system of A interacting particles,

$$H = \sum_{i=1}^A \frac{1}{2m_i} \nabla_i^2 + \sum_{j<i=1}^A v(\mathbf{r}_i, \mathbf{k}_i, \mathbf{r}_j, \mathbf{k}_j) \quad (3.1)$$

where v is the nucleon-nucleon interaction. Now add and subtract a potential field $V(\mathbf{r})$ affecting all particles,

$$\begin{aligned} H &= \sum_i \left[\frac{1}{2m_i} \nabla_i^2 + V(\mathbf{r}_i) \right] + \sum_{j<i} [v(\mathbf{r}_i, \mathbf{k}_i, \mathbf{r}_j, \mathbf{k}_j) - V(\mathbf{r}_i)] \\ &= H_{\text{MF}} + V_{\text{res}} \end{aligned} \quad (3.2)$$

where we have split the Hamiltonian into a spherically symmetric mean-field Hamiltonian H_{MF} in which particles do not interact directly, and the *residual*

interaction V_{res} that can be seen as the new interaction between particles. If the mean-field potential V is chosen carefully, V_{res} can become small enough to be treated perturbationally (if at all).

3.1.1 The Woods-Saxon Potential

For the mean-field potential we will use the established Woods-Saxon potential, visualized in Fig. 3.1, given by

$$V(r) = -V_0 f(r) - 4V_{\text{so}} \mathbf{l} \cdot \mathbf{s} \frac{1}{r} \frac{df}{dr}, \quad (3.3)$$

where

$$f(r) = \left[1 + \exp\left(\frac{r - r_0}{d}\right) \right]^{-1}. \quad (3.4)$$

The parameters are the potential depth V_0 , the spin-orbit coupling strength V_{so} , the range r_0 and the diffuseness d . There are approximate formulas for these values, depending on the number of each kind of nucleon. Alternatively, one can fit the parameters to reproduce experimental energy levels. We will use both approaches.

Note that the spin-orbit coupling term can give either attractive or repulsive contributions, depending on how the angular momenta couples. Recall that

$$\mathbf{l} \cdot \mathbf{s} = \frac{1}{2} (j(j+1) - l(l+1) - s(s+1)) = \begin{cases} l, & \text{if } j = l + \frac{1}{2} \\ -l - 1, & \text{if } j = l - \frac{1}{2} \end{cases}, \quad (3.5)$$

where we have stated the result in the case of one valence nucleon.

3.1.2 Magic Nuclei

The shell model has had some success in reproducing the general features of nuclides[2], especially for lighter nuclei ($A < 50$). It is found that there are magic numbers of nucleons, where the protons or neutrons form complete shells with 0 total angular momentum. Of special interest to us are *doubly magic* nuclei, where both proton and neutron numbers are magic. These nuclei can be very tightly bound, and will therefore interact weakly with nucleons in outer shells. If we add nucleons to a doubly magic nuclei, we can thus treat it as a rigid *core*, interacting with valence neutrons through the mean-field only.

We will consider the special case of core and one valence neutron, two particles with a spherically symmetric potential. We can then perform the

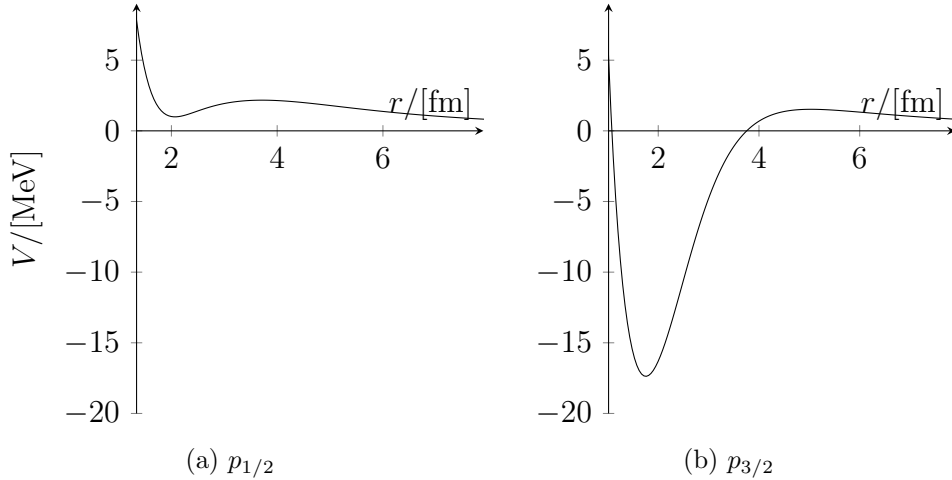


Figure 3.1: The Woods-Saxon potential with centrifugal barrier $l(l+1)/2\mu r^2$ added, for different waves. Parameters $V_0 = 47$ MeV, $r_0 = 2$ fm and $d = 0.65$ fm

standard procedure of reducing the problem to a one-dimensional equation by using the relative coordinate $r = |\mathbf{r}_\alpha - \mathbf{r}_n|$ and the reduced mass

$$\mu = \frac{m_\alpha m_n}{m_\alpha + m_n}. \quad (3.6)$$

3.2 The ${}^5\text{He}$ Nucleus

We choose to study ${}^5\text{He}$, seen as a ${}^4\text{He}$ nucleus and a valence neutron. The ${}^4\text{He}$ nucleus (α particle) is doubly magic, with two $s_{1/2}$ -neutrons and two $s_{1/2}$ -protons forming full shells, creating a stable core. Other doubly magic light nuclei, such as ${}^{16}\text{O}$ and its isotopes, have been studied using methods similar to ours[3], but we will restrict ourselves to ${}^n\text{He}$ nuclei.

Because the s -shell is already filled in ${}^4\text{He}$, the valence neutron of ${}^5\text{He}$ will be a p -wave, with $l = 1$. We see in (3.5) that the $p_{3/2}$ -wave will get a negative net contribution from the total spin-orbit term, also shown in Fig. 3.1. This means that the ground state of ${}^5\text{He}$ will be the $p_{3/2}$ wave, with $p_{1/2}$ an excited state. Both the $p_{3/2}$ and $p_{1/2}$ waves have known resonance states.

The Woods-Saxon parameters will initially be set to standard values to investigate the general behavior of the solutions. The following values are used [3]:

Potential depth	$V_0 = 47 \text{ MeV}$
Spin-orbit coupling strength	$V_{\text{so}} = -7.5 \text{ MeV}$
Range	$r_0 = 2 \text{ fm}$
Diffuseness	$d = 0.65 \text{ fm}$

We later optimize the parameters to match experimentally determined energy levels for ${}^5\text{He}$.

We use the procedures described in Chapter 2 to numerically solve the ${}^5\text{He}$ Schrödinger equation for the $p_{3/2}$ wave. When examining the solutions, we are specifically looking for the ground state resonance.

3.2.1 Harmonic Oscillator Basis

We begin by solving the ${}^5\text{He}$ Schrödinger equation in the HO basis. We plot the solutions in Fig. 3.2 as a function of the range r_0 of the HO potential. All solutions have energies $E > 0$, meaning that they are unbound, scattering states, and thus have unlimited range. However, we see a saddle point in energy for the lowest energy solution when the HO range $r_0 \approx 1 \text{ fm}$, corresponding to radii within the nucleus. The range r_0 is a measure of the

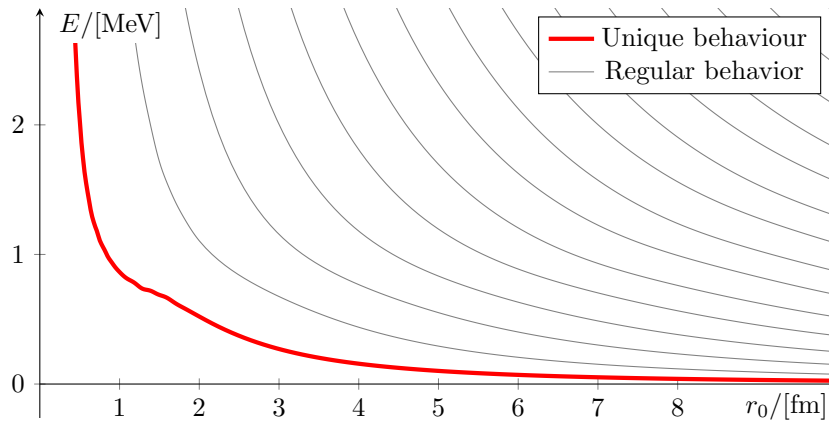


Figure 3.2: The lowest energy eigenvalues of the ${}^5\text{He}$ problem as a function of the HO range r_0 . The lowest energy state behaves differently from the others.

Because the harmonic oscillator consists only of bound states and we are trying to study unbound states, this method cannot take us much further. We will have to switch to a basis with wavefunctions of infinite range to properly describe this system.

3.2.2 Momentum Basis

The momentum basis describes a plane wave, i.e. a free particle, with wave functions of infinite range. Because all ${}^5\text{He}$ solutions appear in the continuum, this basis is better suited to the problem than the HO basis.

Momentum Space Wavefunctions

Solving the Schrödinger equation in the momentum basis gives us momentum eigenfunctions $\phi(k)$, presented in Fig. 3.3. There is a background of wavefunctions peaking at different values of k , and one wavefunction standing out as lower and wider. Let us first discuss the peak-shaped wavefunctions.

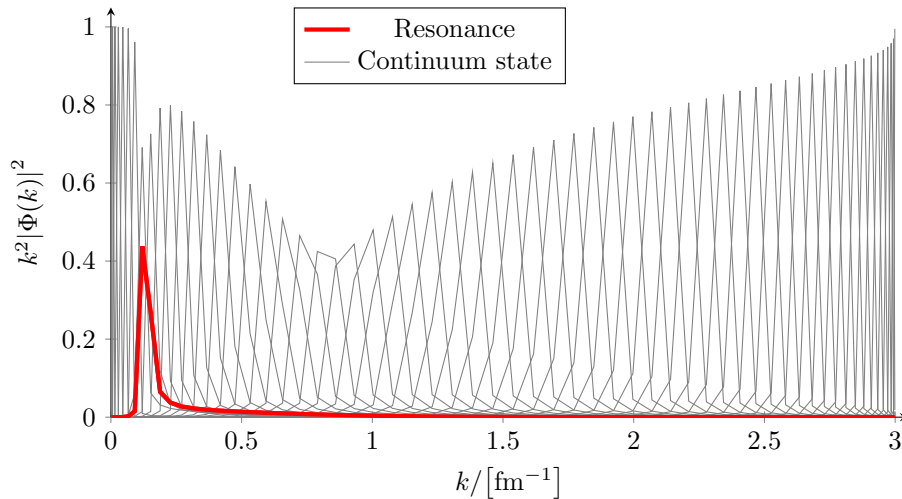


Figure 3.3: ${}^5\text{He}$ momentum probability distributions. The resonance is significantly wider than the surrounding states. We can see a trend toward lower and wider states around 1 fm^{-1} , but it is merely a numerical peculiarity stemming from the normalization.

Recall the relation between wavefunctions in position and momentum representation, (2.21)

$$R(r) = i^l \sqrt{\frac{2}{\pi}} \int_0^\infty dk k^2 \phi(k) j_l(kr). \quad (3.7)$$

A wavefunction peaking at a single value k_i corresponds to a radial wavefunction

$$R_i(r) = i^l \sqrt{\frac{2}{\pi}} j_l(k_i r) \quad (3.8)$$

The spherical bessel functions $j_l(k_i r)$ are eigensolutions to the Schrödinger equation for free particles with spherical symmetry. We can thus conclude that the peak-shaped solutions correspond to free particles. This is not unexpected as we are dealing with an open quantum system that only marginally perturbs passing particles, explaining why we find unbound solutions corresponding to each value of k used in the discretized basis.

The unique state peaks at $k = 0.17 \text{ fm}^{-1}$ and is wider than the surrounding states. The Heisenberg uncertainty relation tells us that a less well-defined momentum corresponds to a more well-defined position. Consequently, this state should correspond to a localized wavefunction, which is what we expect from a resonance.

Position Space Wavefunctions

To investigate the relation between the hypothesized resonance solution and a bound solution, we increase the depth of the potential to $V_0 = 70 \text{ MeV}$, and successively decrease the depth until there is no bound state. This is documented in Fig. 3.4, where the radial probability distributions $r^2|R(r)|^2$ are plotted for the widest momentum wavefunction together with an arbitrary unbound state. With a deep potential, the bound state wavefunction quickly tends to zero outside the potential well. As we decrease the depth below a certain threshold, the potential well no longer supports the bound state ($E > 0$), but the wavefunction remains localized. This is the region of the ${}^5\text{He}$ depth (47 MeV) where we should find the resonance. When V_0 is decreased even further, the resonance disappears.

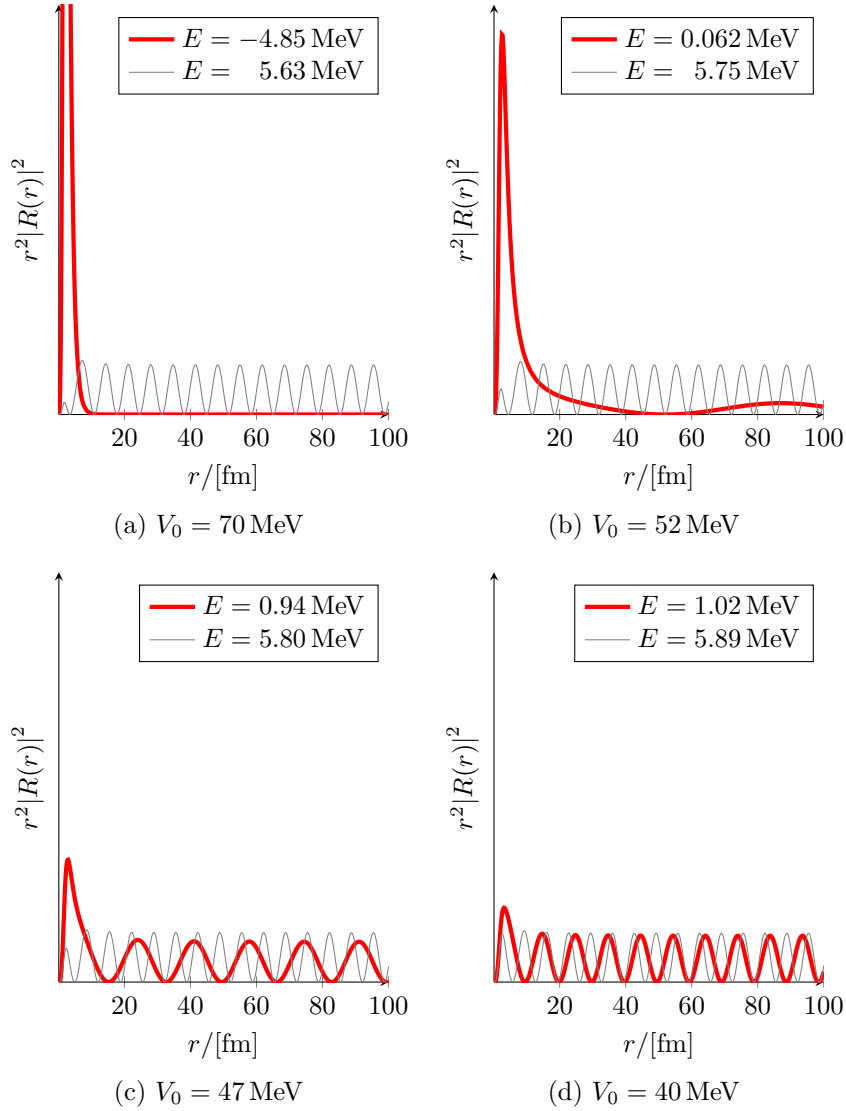


Figure 3.4: ${}^5\text{He}$ wavefunctions for varying potential depth. Plotted are the unique localized solution (thick line) and, for comparison, an arbitrary continuum solution (thin line). With a deep potential $V_0 = 70$ MeV there is a strongly bound state, which gets weaker as the potential depth is decreased. At $V_0 = 52$ MeV the wavefunction is highly localized, yet the energy lie in the continuum, a sign of resonance. There is still a clearly localized state for $V_0 = 47$ MeV, but at $V_0 = 40$ MeV it is practically indistinguishable from the other continuum states.

Chapter 4

The Complex-Momentum Basis

In Chapter 3 we studied the ${}^5\text{He}$ system and found a special state in the continuum, the resonance. We will in this chapter detail a method of extending the momentum basis to the complex momentum plane, which gives a more complete description of resonances. We also state the important Berggren completeness relation. The ${}^5\text{He}$ problem is examined once more using the complex-momentum basis and we fit the model parameters to experimental resonance data.

4.1 The Complex Momentum Plane

When solving the Schrödinger equation in the momentum basis, we know that the solutions form a complete basis, expressed as a completeness relation

$$\sum_{\text{bound}} |E_n\rangle\langle E_n| + \int_0^\infty dk k^2 |E_k\rangle\langle E_k| = 1, \quad (4.1)$$

where E_n are discrete bound states and E_k are continuous.

If we relate the energies E to momenta k as

$$E = \frac{\hbar^2 k^2}{2\mu} \quad \text{or} \quad k = \frac{\sqrt{2\mu E}}{\hbar}, \quad (4.2)$$

we can plot the solutions as k in the complex plane, see Fig. 4.1. We then expect bound states, with $E < 0$, to be represented by discrete k along the imaginary axis—whereas unbound states with $E > 0$, are found continuously along the real axis. Resonance states, with complex $E = E_0 - i\Gamma/2$, would by this argument appear somewhere in the fourth quadrant.

It is known that bound and resonant states indeed correspond to poles in the complex momentum plane at $k = \sqrt{2\mu E}/\hbar$. The details of this is treated

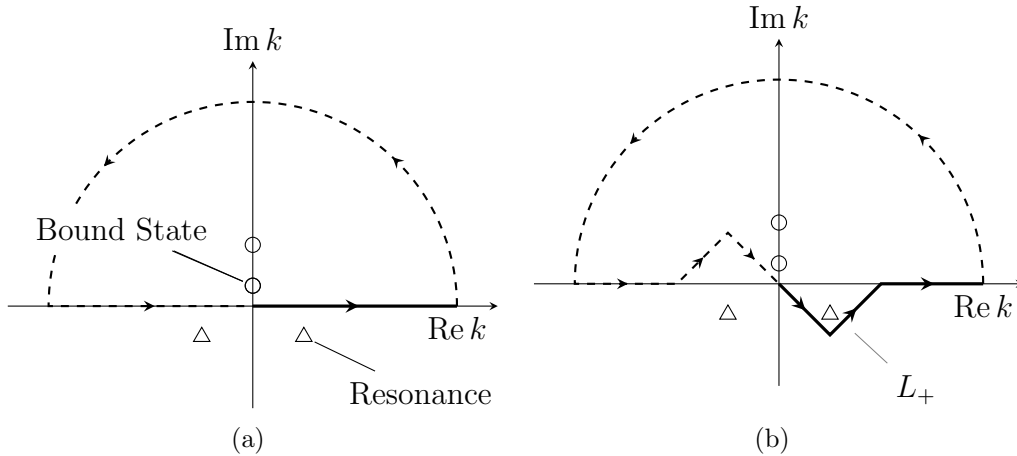


Figure 4.1: The complex k -plane. The circles represent bound states and the triangles resonant states. Note the mirroring of the states in the imaginary axis.

in scattering theory, and is beyond the scope of this thesis. We interpret the bound and resonant k as complex poles and treat the unbound continuum as a contour, mirrored in the imaginary axis, encircling the upper half plane (Fig. 4.1a).

The integral to be evaluated along the contour is the radial momentum space Schrödinger equation

$$\frac{k^2}{2\mu}\phi(k) + \int_0^\infty dk' k'^2 V(k, k')\phi(k') = E\phi(k). \quad (4.3)$$

The result of a contour integration depends on the poles it encircles by the residue theorem. The contour in Fig. 4.1a encircles the bound states, but not the resonance. We suspect a deformation of the contour, such that it goes below the resonance, might have an effect on the solutions.

4.1.1 The Berggren Completeness Relation

In fact, this is correct, and was proven in 1968 by Berggren [1]. The contour, dubbed L_+ , can be deformed to surround the resonance poles, as illustrated in Fig. 4.1b. The continuum states along L_+ combined with the encircled bound and resonant states form a complete basis, the *Berggren basis*. This result can be stated succinctly with the *Berggren completeness relation* (compare

with (4.1))

$$\sum_{\substack{\text{bound} \\ \text{resonant}}} |E_n\rangle\langle E_n| + \int_{L_+} dk k^2 |E_k\rangle\langle E_k| = 1. \quad (4.4)$$

This is an important result, because of the inclusion of the resonances in the basis. The Berggren basis is what allows us to find resonances in systems with more particles.

An observant reader may have noticed that the resonant poles in Section 4.1 are mirrored in the imaginary axis and that the contour has a shadow on the left half plane. Berggren showed that this symmetry allows us to restrict ourselves to the contour segment from 0 to ∞ . However, doing this leads to a scalar product *without conjugation* that must be used

$$\langle\phi|\phi'\rangle = \int_0^\infty dk k^2 \phi(k)\phi'(k). \quad (4.5)$$

Naturally, this also affects the norm.

4.2 ^5He Revisited

With the complex-momentum basis we can continue our study of the ^5He system. We use the same Woods-Saxon parameters as before, but now use a complex contour. The solutions will be examined in a similar fashion to Chapter 3.

4.2.1 The Discretized Complex Contour

We deform the previously real contour by a triangle-shaped downward extrusion, as in Fig. 4.2. The tip of the triangle is placed below the expected position of the resonance pole. To use the contour in computations it has to be discretized, as before in Section 2.3.1. We use the Gauss-Legendre quadrature, but now consider each segment of the contour separately: This requires us to rescale the evaluation points and weights between each pair of complex endpoints according to Appendix B.1. The discretized contour is seen in Fig. 4.2. Note the concentration of points near the ends of each segment, characteristic of the Gauss-Legendre quadrature.

The discretized Schrödinger equation (2.27) is unchanged from before

$$H'_{ij} = \frac{k_i^2}{2\mu} \delta_{ij} + \sqrt{w_i w_j} k_i k_j V_{ij}, \quad (4.6)$$

but now the k and w are complex. However, when normalizing the obtained eigenvectors, one must make sure to use the new scalar product defined in (4.5).

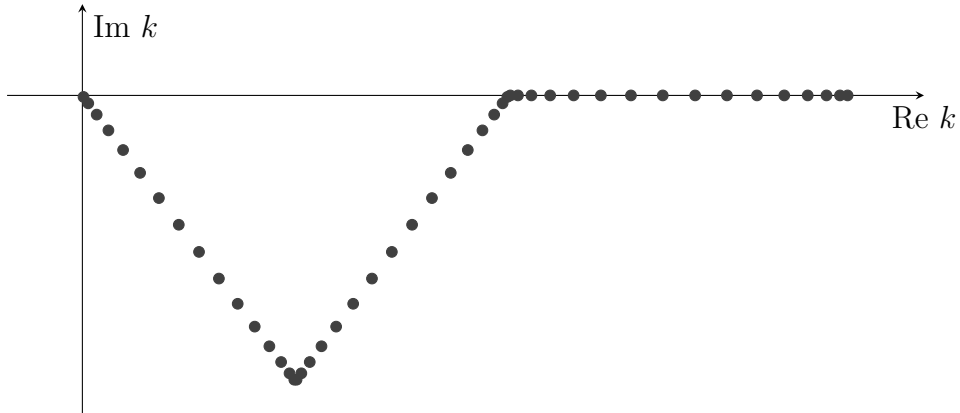


Figure 4.2: A schematic picture of the discretized complex contour. The points are distributed on each segment according to the Gauss-Legendre quadrature rule.

4.2.2 The ${}^5\text{He}$ Resonances

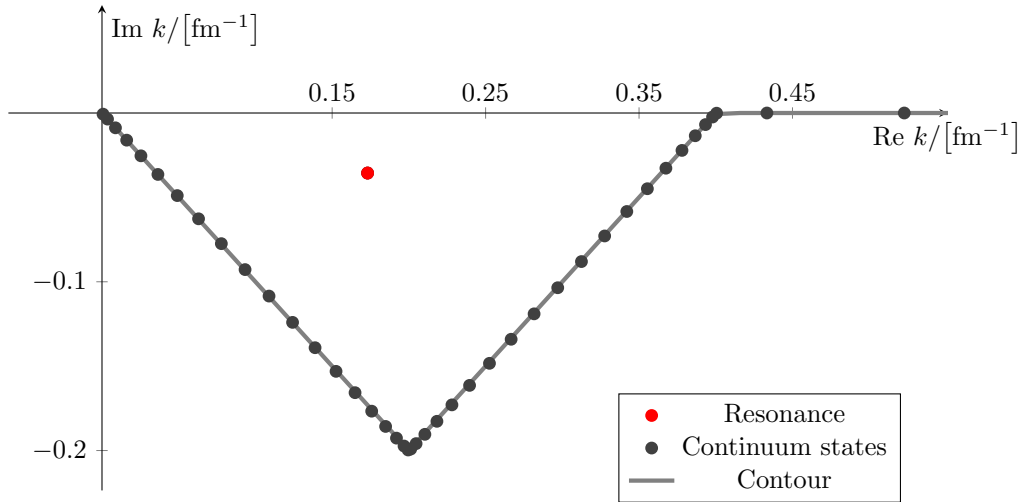
We expect the position k_r of the resonance poles to be fairly close to the experimental data in Table 4.2, hence we choose a triangular contour that extends below the expected position. Table 4.1 presents the poles and the contours used to identify them.

We solve the Schrödinger equation using the contours and represent the energy solutions by their momenta $k = \sqrt{2\mu E}$. The result for the $p_{3/2}$ wave is shown in Fig. 4.3a. We see that most solutions follow the contour, corresponding to non-resonant continuum states, similarly to the real case. There is one solution that does not lie on the contour, however. It has $k = (0.173 - 0.0357i) \text{ fm}^{-1}$, which is reasonably close to what we expected for the resonance. If we have indeed found the resonance, we expect it to be unchanged when the contour is varied. In Fig. 4.3b, a rectangular contour is used instead of the triangular, yet the pole is completely stable. We also found that we could vary the downward extrusion of the contour to some extent without the resonance pole moving. But with sufficiently large imaginary parts, the matrix element integrals started to diverge. Barring such numerical errors, we found that any contour that runs below and not too close to the

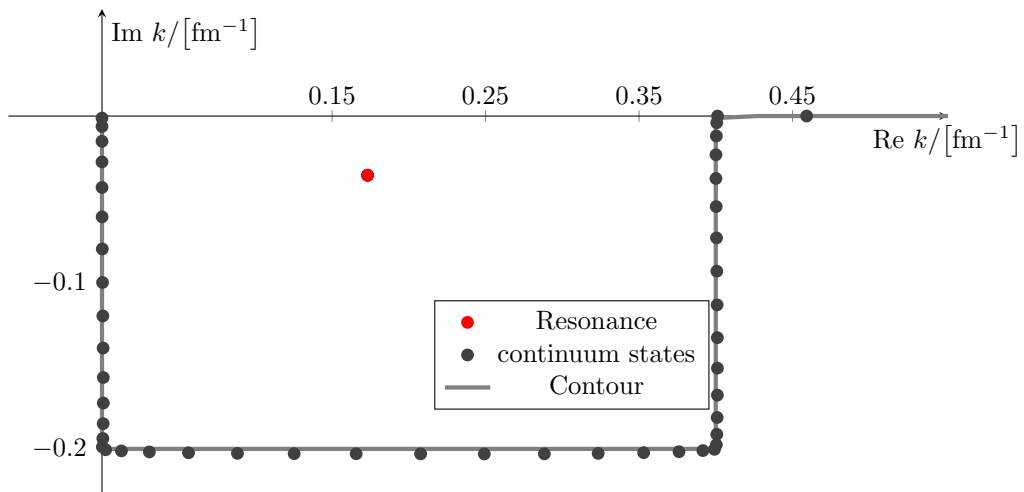
Table 4.1: Contours used to identify ${}^5\text{He}$ resonances.

Wave	Experimental k_r	Computed k_r	Contour vertices
$p_{3/2}$	$0.179 - 0.0349i$	$0.173 - 0.0357i$	$(0, 0) \rightarrow (0.17, -0.2) \rightarrow (0.34, 0) \rightarrow (2.5, 0) \text{ fm}^{-1}$
$p_{1/2}$	$0.327 - 0.164i$	$0.331 - 0.170i$	$(0, 0) \rightarrow (0.35, -0.4) \rightarrow (0.7, 0) \rightarrow (2.5, 0) \text{ fm}^{-1}$

pole gives a stable resonance solution.



(a) Triangle Contour



(b) Rectangular Contour

Figure 4.3: Momentum solutions for a ${}^5\text{He}$ $p_{3/2}$ wave for different contours. The resonance is located at $0.173 - 0.0356i$ for both contours. we have used $V_0 = 47 \text{ MeV}$ with $k_{max} = 5 \text{ fm}^{-1}$ with 60 points on both contours.

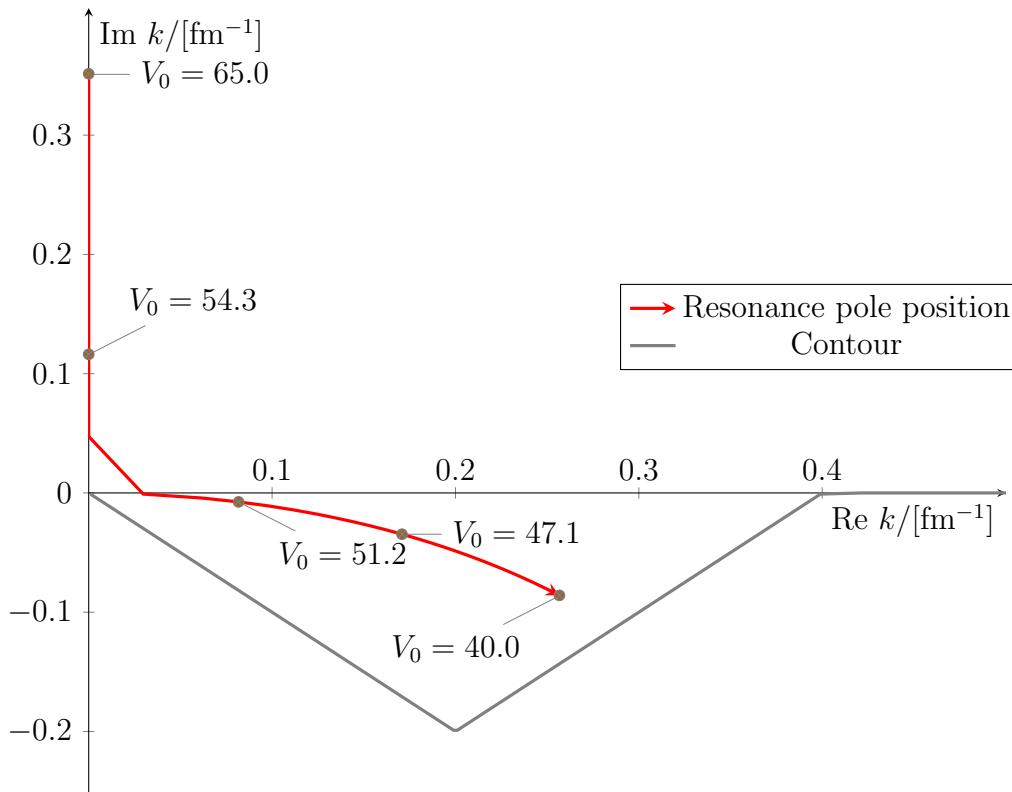
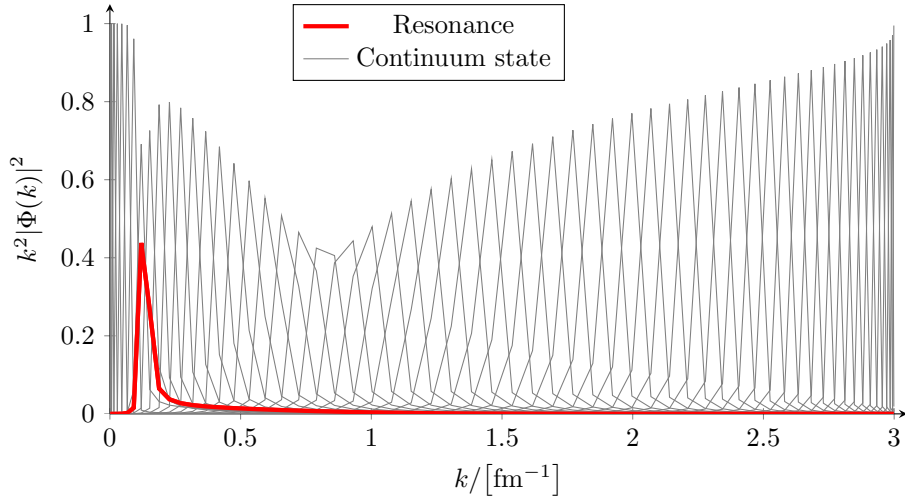


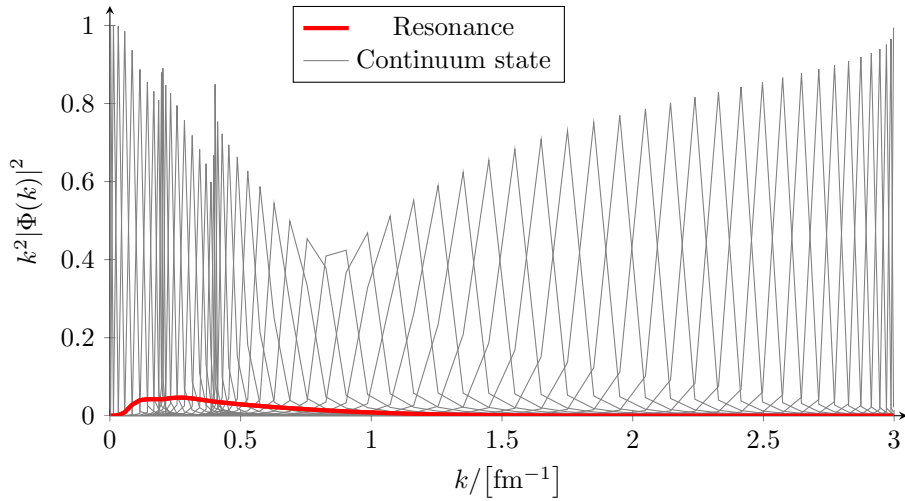
Figure 4.4: The position of the resonance pole as a function of V_0 . The pole begins at 70 MeV as a bound state on the imaginary axis, gradually becomes less and less bound, jumps into the fourth quadrant ($V_0 \approx 52$ MeV), passes the ${}^5\text{He}$ resonance and continues further down and to the right.

Momentum Space Wavefunctions

As in Chapter 3 we can study the momentum wavefunctions obtained in the diagonalization. Figure 4.5 shows the momentum distribution of an arbitrary unbound solution and the resonance. We also show the corresponding situation when using the real basis, for comparison. Note how the resonance wavefunction is much more distinguished in the complex basis. The unbound solution still correspond to one definite (now complex) momentum. On the other hand, the resonance has a wide distribution, reflecting the localized nature of the solution (remember Heisenberg—a wide momentum wavefunction allows a localized position wavefunction). This also allows for automatically finding the resonance among a large set of solutions by singling out the one with the widest (or lowest) wavefunction.



(a) Momentum space wavefunctions with a real contour.



(b) Momentum space wavefunctions with a complex contour.

Figure 4.5: ${}^5\text{He}$ momentum probability distributions for a real and complex contour. The resonance is more prominent when solving along the complex contour but is significantly wider than the surrounding states in both cases. Both contours comprise 60 points in total, but the points in the complex contour are concentrated near the origin, stemming from the Gauss-Legendre distribution on the individual segments.

Varying the Potential Depth

We repeat the procedure from Section 3.2.2, lowering the potential well to 70 MeV and increasing it gradually, but we now plot the position of the

bound/resonance pole in the complex plane. Figure 4.4 we see how the pole starts on the imaginary axis at $V_0 = 70$ MeV. It then moves downwards, becoming less and less strongly bound. At $V_0 \approx 52$ MeV the pole jumps to the fourth quadrant, becoming a resonance. As the potential well grows even less attractive, we see that both the binding energy E_0 and the width Γ of the resonance increases.

4.2.3 Fitting to Experimental Resonance Data

Having studied the solutions and verified that we have found the resonances, we now proceed to fit our model of ${}^5\text{He}$ to experimental data. The data, taken from [4], is presented in Table 4.2 along with simulated results. Fitting the Woods-Saxon parameters after the four experimental data points resulted in optimal values $V_0 = 47.05$ MeV and $V_{\text{so}} = -7.04$ MeV.

Table 4.2: Experimental ${}^5\text{He}$ resonance data [4] and computed values with fitted Woods-Saxon parameters $V_0 = 47.05$ MeV and $V_{\text{so}} = -7.04$ MeV. All values are in MeV.

Wave	Experimental data		Computed values	
	E_0	Γ	E_0	Γ
$p_{3/2}$:	0.798	0.648	0.783	0.695
$p_{1/2}$:	2.068	5.57	2.111	5.560

Chapter 5

Many-Body Theory and Implementation

We have solved the ${}^5\text{He}$ nuclear two-body problem and studied its resonances. The next step is to add another neutron and subsequently solve the three-body problem. However, while the two-body problem is reducible to a radial one-dimensional problem, the general many-body problem is not. Instead, we need to use a single particle (sp) basis to construct many-body states. This chapter covers the construction of such states.

First, Section 5.1 discusses the mathematical consequences of identical, indistinguishable particles, focusing on fermions. This is followed in Section 5.2 by a short introduction to the second quantization formalism, which allows calculations with an arbitrary number of particles. The line of reasoning as well as the notation of these sections is adapted from [5], to facilitate further reading for the interested reader. With the same intention, the style of [2] is employed in Section 5.3 where the concept of angular momentum coupling is briefly explained. Finally, in Section 5.4 we discuss the use of second quantization in computations and present a simple implementation for fermions.

5.1 Identical Particles

A quirk of quantum mechanics is that particles that look identical *are* identical. For example, consider the nucleons in a nucleus. The neutrons and protons have different charge, and can thus be told apart, but distinguishing between individual neutrons is impossible. This has to be taken into consideration when dealing with many-body states of identical particles, as we will see.

We begin with an orthonormal single particle basis $|\alpha_i\rangle$, where α_i represents

all the quantum numbers that describe the state. Next, consider N identical particles, expressed in this basis. We form product states

$$|\alpha_1\alpha_2\dots\alpha_N\rangle \equiv |\alpha_1\rangle \otimes |\alpha_2\rangle \otimes \dots \otimes |\alpha_N\rangle = |\alpha_1\rangle|\alpha_2\rangle\dots|\alpha_N\rangle, \quad (5.1)$$

which, by the orthonormality of the $|\alpha\rangle$, are orthonormal as well

$$(\alpha_1\alpha_2\dots\alpha_N|\alpha'_1\alpha'_2\dots\alpha'_N) = \delta_{\alpha_1\alpha'_1}\delta_{\alpha_2\alpha'_2}\dots\delta_{\alpha_N\alpha'_N}. \quad (5.2)$$

Let us assume that the system of identical particles can be described by some linear combinations of these basis states, denoted

$$|\alpha_1\alpha_2\dots\alpha_N\rangle. \quad (5.3)$$

Since the particles are identical, and thus indistinguishable, we require the norm of the state to be unchanged when swapping the quantum numbers of two particles β and γ

$$\begin{aligned} \langle\alpha_1\dots\beta\dots\gamma\dots\alpha_N|\alpha_1\dots\beta\dots\gamma\dots\alpha_N\rangle \\ = \langle\alpha_1\dots\gamma\dots\beta\dots\alpha_N|\alpha_1\dots\gamma\dots\beta\dots\alpha_N\rangle \end{aligned} \quad (5.4)$$

These states can therefore only differ in phase $e^{i\varphi}$, and since another swap will bring us back to the original state, the phase has to be either $e^{i\varphi} = 1$ or $e^{i\varphi} = -1$. Symmetric states with no phase change describe *bosons*, whereas antisymmetric states that change sign describe *fermions*. In this thesis all sp states will be fermionic, hence we do not treat the bosonic case.

5.1.1 Antisymmetric Fermion states

We have now established that our fermion many-body states are a linear combination of product states that satisfy

$$|\alpha_1\dots\alpha_i\dots\alpha_j\dots\alpha_N\rangle = -|\alpha_1\dots\alpha_j\dots\alpha_i\dots\alpha_N\rangle. \quad (5.5)$$

For example, in the case of two particles, the correctly normalized antisymmetric state is

$$|\alpha_1\alpha_2\rangle = \frac{1}{\sqrt{2}}(|\alpha_1\alpha_2\rangle - |\alpha_2\alpha_1\rangle). \quad (5.6)$$

We will henceforth use the angular ket notation $|\dots\rangle$ for antisymmetric states, as opposed to $|\dots\rangle$ for product states.

Let us ponder that two fermions occupy the same state. Exchanging the two particles and flipping the sign would then result in

$$|\alpha\alpha\alpha_1\dots\alpha_N\rangle = -|\alpha\alpha\alpha_1\dots\alpha_N\rangle \quad (5.7)$$

which can only be true if both states are 0. We conclude that two fermions can never occupy the same state, commonly referred to as the *Pauli Principle*.

It is important to note that states with permuted quantum numbers, such as the states $|\alpha_1\alpha_2\rangle$ and $|\alpha_2\alpha_1\rangle$, represent the same physical state, as they only differ in sign (phase). This means that we have to make sure not to double count these states. We can do this by requiring that the sp states always appear in the same order in the ket. If they do not, we permute two sp states at a time until the correct ordering is reached

$$\begin{aligned}
|\alpha_i\alpha_1 \dots \alpha_{i-1}\alpha_{i+1} \dots \alpha_N\rangle &= -|\alpha_1\alpha_i \dots \alpha_{i-1}\alpha_{i+1} \dots \alpha_N\rangle \\
&= \dots \\
&= (-1)^{i-2}|\alpha_1 \dots \alpha_i\alpha_{i-1}\alpha_{i+1} \dots \alpha_N\rangle \\
&= (-1)^{i-1}|\alpha_1 \dots \alpha_{i-1}\alpha_i\alpha_{i+1} \dots \alpha_N\rangle.
\end{aligned} \tag{5.8}$$

With a well-defined ordering orthonormality of the normalized antisymmetric states can be stated simply

$$\langle \alpha_1\alpha_2 \dots \alpha_N | \alpha'_1\alpha'_2 \dots \alpha'_N \rangle = \delta_{\alpha_1\alpha'_1} \delta_{\alpha_2\alpha'_2} \dots \delta_{\alpha_N\alpha'_N}. \tag{5.9}$$

5.2 Second quantization

So far we've looked at a system with a fixed number of particles, but we want to work with a system hosting an arbitrary number of identical particles. The *second quantization* formalism lets us do this by introducing the *Fock space*, a direct sum of Hilbert spaces of 0, 1, 2, ... particles. This means that a state in Fock space, a *Fock state*, can contain any number of particles and that Fock states with different number of particles are orthogonal.

A disclaimer is in place here: while we introduce this powerful concept, we do not make full use of it in this thesis. It should instead be considered as a stepping stone for readers wishing to expand on the systems and methods that we do use.

5.2.1 Creation and Annihilation Operators

The simplest Fock state is the *vacuum state* $|0\rangle$, which describes a system with no particles. All other states can be created from the vacuum state using the *creation operator* a_α^\dagger , which adds a particle with quantum numbers α to a state

$$a_\alpha^\dagger |\alpha_1\alpha_2 \dots \alpha_N\rangle = |\alpha\alpha_1\alpha_2 \dots \alpha_N\rangle. \tag{5.10}$$

The resulting state will not necessarily be ordered, and the ordering might contribute a sign:

$$a_{\alpha_i}^\dagger |\alpha_1 \alpha_2 \dots \alpha_{i-1} \alpha_{i+1} \dots \alpha_N\rangle = (-1)^{i-1} |\alpha_1 \alpha_2 \dots \alpha_{i-1} \alpha_i \alpha_{i+1} \dots \alpha_N\rangle. \quad (5.11)$$

Note that when a_α^\dagger acts on a state that already contains a particle with quantum numbers α , the result is 0, because of the Pauli principle

$$a_\alpha^\dagger |\alpha \alpha_1 \alpha_2 \dots \alpha_N\rangle = 0. \quad (5.12)$$

The adjoint of the creation operator is called the *annihilation operator* a_α . It can be shown to have the opposite effect, removing a particle, when acting on a state

$$a_\alpha |\alpha \alpha_1 \alpha_2 \dots \alpha_N\rangle = |\alpha_1 \alpha_2 \dots \alpha_N\rangle. \quad (5.13)$$

Here, too, a sign might appear from the ordering

$$a_{\alpha_i} |\alpha_1 \alpha_2 \dots \alpha_{i-1} \alpha_i \alpha_{i+1} \dots \alpha_N\rangle = (-1)^{i-1} |\alpha_1 \alpha_2 \dots \alpha_{i-1} \alpha_{i+1} \dots \alpha_N\rangle. \quad (5.14)$$

Analogous to a_α^\dagger , when a_α acts on a state that does not contain a particle with the quantum numbers α , the result is 0

$$a_\alpha |\alpha_1 \alpha_2 \dots \alpha_N\rangle = 0. \quad (5.15)$$

5.2.2 General Operators in Fock Space

We can now express the state of an arbitrary number of particles, but to have any use of the states we also need to express operators such as the Hamiltonian in the Fock space formalism. A general operator has can in Fock space be expressed using the creation and annihilation operators. The Fock space equivalent of an operator is able act on a state with an arbitrary number of particles. We will only treat one- and two-body operators here, as they are sufficient for our purposes.

One-Body Operators

A one-body operator H_1 which acts on a single sp state, is represented by the Fock space operator

$$\hat{H}_1 = \sum_{\alpha\beta} \langle \alpha | H_1 | \beta \rangle a_\alpha^\dagger a_\beta. \quad (5.16)$$

It is important to note that while the sum runs over the complete set of sp states twice, only a few terms will be non-zero, because of the operator rules in (5.12) and (5.15).

If the sp-states are eigenstates to the one-body operator

$$H_1|\alpha\rangle = h_\alpha|\alpha\rangle \quad (5.17)$$

the matrix elements only exist on the diagonal, when $\alpha = \beta$, and we get

$$\hat{H}_1 = \sum_{\alpha} \langle \alpha | H_1 | \alpha \rangle a_{\alpha}^{\dagger} a_{\alpha}. \quad (5.18)$$

The many-body matrix element becomes

$$\begin{aligned} \langle a_1 \dots a_N | \hat{H}_1 | b_1 \dots b_N \rangle &= \sum_{\alpha} \langle \alpha | H_1 | \alpha \rangle \langle a_1 \dots a_N | a_{\alpha}^{\dagger} a_{\alpha} | b_1 \dots b_N \rangle \\ &= \sum_{i=1}^N \langle a_i | H_1 | a_i \rangle \langle \alpha_1 \dots \alpha_N | \alpha'_1 \dots \alpha'_N \rangle \\ &= (h_1 + \dots + h_N) \delta_{a_1 b_1} \dots \delta_{a_N b_N}, \end{aligned} \quad (5.19)$$

the sum of the eigenvalues of the sp states in the bra or ket, but only if the bra and ket are the same. The Fock space operator \hat{H}_1 is thus also diagonal.

Two-Body Operators

A two-body operator in Fock space becomes

$$\hat{H}_2 = \frac{1}{2} \sum_{\alpha\beta\gamma\delta} (\alpha\beta | H_2 | \gamma\delta) a_{\alpha}^{\dagger} a_{\beta}^{\dagger} a_{\delta} a_{\gamma}. \quad (5.20)$$

Note that the ordering of the γ and δ is different for the product states and the operators, so-called *normal ordering*. The factor $1/2$ stems from the fact that

$$(\alpha\beta | H_2 | \gamma\delta) = (\beta\alpha | H_2 | \delta\gamma), \quad (5.21)$$

and we are counting both.

We can also express \hat{H}_2 using matrix elements between antisymmetric states

$$\langle \alpha\beta | H_2 | \gamma\delta \rangle = (\alpha\beta | H_2 | \gamma\delta) - (\alpha\beta | H_2 | \delta\gamma), \quad (5.22)$$

but we will have to add another factor $1/2$ to compensate for double counting

$$\hat{H}_2 = \frac{1}{4} \sum_{\alpha\beta\gamma\delta} \langle \alpha\beta | H_2 | \gamma\delta \rangle a_{\alpha}^{\dagger} a_{\beta}^{\dagger} a_{\delta} a_{\gamma}. \quad (5.23)$$

The double counting can be avoided, however, by taking into account the ordering of the states

$$\hat{H}_2 = \sum_{\substack{\alpha < \beta \\ \gamma < \delta}} \langle \alpha\beta | H_2 | \gamma\delta \rangle a_{\alpha}^{\dagger} a_{\beta}^{\dagger} a_{\delta} a_{\gamma}. \quad (5.24)$$

For the special case of two particles we have

$$\begin{aligned}
\langle ab|\hat{H}_2|cd\rangle &= \sum_{\substack{\alpha<\beta \\ \gamma<\delta}} \langle \alpha\beta|H_2|\gamma\delta\rangle \langle ab|a_\alpha^\dagger a_\beta^\dagger a_\delta a_\gamma|cd\rangle \\
&= \sum_{\substack{\alpha<\beta \\ \gamma<\delta}} \langle \alpha\beta|H_2|\gamma\delta\rangle \delta_{\alpha a} \delta_{\beta b} \delta_{\gamma c} \delta_{\delta d} \\
&= \langle ab|H_2|cd\rangle,
\end{aligned} \tag{5.25}$$

as expected.

5.3 Angular Momentum Coupling

We have now developed the theory we need to solve actual many-body problems. Before applying these methods, however, we will discuss the concept of angular momentum coupling. This corresponds to making a change of basis, using the rotational symmetry of problems to make the Hamiltonian matrix block diagonal and significantly reducing its size. In principle, coupling is not necessary to solve many-body problems, but its an invaluable tool. We will limit the discussion to coupling of two particles, as we never work with more particles here. A more complete description is found in [2].

5.3.1 The Two-Particle Coupled Basis

In previous Chapters we have studied single-particle states on the form $|Ejm\rangle$, where we let the quantum number E represent all quantum numbers needed to uniquely specify a state. From these we would form product states

$$|E_1 j_1 m_1, E_2 j_2 m_2\rangle = |E_1 j_1 m_1\rangle \otimes |E_2 j_2 m_2\rangle \tag{5.26}$$

that are eigenstates to the operators $\mathbf{J}_1 = \mathbf{J} \otimes \mathbf{1}$ and $\mathbf{J}_2 = \mathbf{1} \otimes \mathbf{J}$.

One often studies systems where the total angular momentum $\mathbf{J} = \mathbf{J}_1 + \mathbf{J}_2$ is conserved, but the individual angular momenta \mathbf{J}_1 and \mathbf{J}_2 are not. Conservation of \mathbf{J} is equivalent to the entire system being symmetric under rotation, while \mathbf{J}_1 and \mathbf{J}_2 will only be conserved if one of the particles can be rotated independently of the other, without affecting the solutions. This is rarely the case when studying directly interacting particles. It is then convenient to switch to a basis where the total angular momentum is well defined, but the individual momenta are not.

We introduce the *coupled* basis with states $|E_1 j_1, E_2 j_2; JM\rangle$ meant to be read as: the first particle is described by the quantum numbers $E_1 j_1$, the

second by E_2j_2 , and they together have a total angular momentum JM (the M is sometimes left out). The coupled states are related to the uncoupled by

$$|E_1j_1, E_2j_2; JM\rangle = \sum_{m_1, m_2} c_{m_1m_2} |E_1j_1m_1, E_2j_2m_2\rangle. \quad (5.27)$$

where $c_{m_1m_2}$ are the *Clebsch-Gordan coefficients* (which also depend on j_1, j_2, J and M , though this is suppressed for brevity). There are known expressions for these, and values can be found in standard tables or calculated in a fairly straight-forward way. A more in-depth treatment of the coefficients can be found in [2].

Working with matrix elements between coupled basis states is called working in the *coupled scheme* or *J-scheme*. If we study a system with rotational symmetry, the Hamiltonian will be block diagonal in J and M , meaning that working in the coupled scheme will be much more efficient.

5.3.2 Antisymmetrizing the Coupled Basis

Since we are studying fermions, we need to use basis states that are antisymmetric with respect to exchange of all quantum numbers. Using the m symmetry property of the Clebsch-Gordan coefficients,

$$c_{m_2m_1} = (-1)^{j_1+j_2-J} c_{m_1m_2} \quad (5.28)$$

we can see that

$$\begin{aligned} |E_2j_2, E_1j_1; JM\rangle &= \sum_{m_1, m_2} c_{m_1m_2} |E_2j_2m_1, E_1j_1m_2\rangle \\ &= (-1)^{j_1+j_2-J} \sum_{m_1, m_2} c_{m_1m_2} |E_2j_2m_2, E_1j_1m_1\rangle \end{aligned} \quad (5.29)$$

Hence it is possible to form the antisymmetric basis vector

$$\begin{aligned} |E_1j_1E_2j_2; JM\rangle &= \frac{1}{\sqrt{2}} \left(|E_1j_1E_2j_2; JM\rangle - (-1)^{j_1+j_2-J} |E_2j_2E_1j_1; JM\rangle \right) \\ &= \sum_{m_1, m_2} c_{m_1m_2} |E_1j_1m_1, E_2j_2m_2\rangle. \end{aligned} \quad (5.30)$$

Consider the case where both particles occupy the same orbital, $E_1j_1 = E_2j_2 = Ej$. Since, for fermions, j is a half-integer we have $(-1)^{j_1+j_2-J} = -(-1)^J$ and the result is

$$|(Ej)^2; JM\rangle = \frac{1 + (-1)^J}{\sqrt{2}} |(Ej)^2; JM\rangle. \quad (5.31)$$

We see that this state is equal to zero for J odd. However, for J even, we find that the norm

$$\langle (Ej)^2; JM | (Ej)^2; JM \rangle = 2 \quad (5.32)$$

meaning that we have to normalize these states with an additional factor $1/\sqrt{2}$. We can write this result succinctly as

$$|ab; JM\rangle = \mathcal{N}_{ab} \sum_{m_1, m_2} c_{m_1 m_2} |E_1 j_1 m_1, E_2 j_2 m_2\rangle \quad (5.33)$$

$$\mathcal{N}_{ab} = \frac{\sqrt{1 + (-1)^J \delta_{ab}}}{1 + \delta_{ab}} \quad (5.34)$$

where we have used the notation (a, b) for $(E_1 j_1, E_2 j_2)$.

5.3.3 Coupled Matrix Elements

When solving problems in practice we need to form matrix elements in the coupled basis. Using the notation $|E_1 E_2\rangle = |E_1 j_1 E_2 j_2; JM\rangle$ for short, we would have

$$\langle E_1 E_2 | \hat{H} | E'_1 E'_2 \rangle = \mathcal{N}_{E_1 E_2} \mathcal{N}_{E'_1 E'_2} \sum_{m_1, m_2} \sum_{m'_1, m'_2} \overline{c_{m_1 m_2}} c_{m'_1 m'_2} \langle E_1 m_1 E_2 m_2 | \hat{H} | E'_1 m'_1 E'_2 m'_2 \rangle \quad (5.35)$$

meaning that the matrix elements in the new basis are given by linear combinations of the elements in uncoupled basis. We only need to evaluate the elements $\langle E_1 m_1 E_2 m_2 | \hat{H} | E'_1 m'_1 E'_2 m'_2 \rangle$, and be done. Since we do not know what the two-body interaction may look like, we cannot do a general treatment of that contribution. Instead we focus on the one-body term, which was treated in (5.19). There is a subtle detail, however, that needs to be addressed.

Even if both single-particle states are the same in the coupled basis $E_1 = E_2 = E$, we will still sum over all m_1, m_2 in the ket $|Em_1 Em_2\rangle$, meaning that we will *not* order our states in that calculation. Instead (5.19) will read

$$\langle E_1 m_1 E_2 m_2 | \hat{H}_1 | E'_1 m'_1 E'_2 m'_2 \rangle = (E_1 + E_2) \delta_{E_1 E'_1} \delta_{E_2 E'_2} (\delta_{m_1 m'_1} \delta_{m_2 m'_2} - \delta_{E_1 E_2} \delta_{m_1 m'_2} \delta_{m_2 m'_1}). \quad (5.36)$$

Inserted into (5.35), this results in

$$\begin{aligned} \langle E_1 E_2 | \hat{H}_1 | E'_1 E'_2 \rangle &= \mathcal{N}_{E_1 E_2} \mathcal{N}_{E'_1 E'_2} (E_1 + E_2) (1 + \delta_{E_1 E_2} (-1)^J) \delta_{E_1 E'_1} \delta_{E_2 E'_2} \\ &= \frac{1 + (-1)^J \delta_{E_1 E_2}}{1 + \delta_{E_1 E_2}} \delta_{E_1 E'_1} \delta_{E_2 E'_2} (E_1 + E_2), \end{aligned} \quad (5.37)$$

where the identity $\sum_{m_1, m_2} |c_{m_1 m_2}|^2 = 1$ was used. Remember that E_1 is short for all quantum numbers specifying that single-particle state.

5.4 Second Quantization Implementation

To use the Fock space formalism in numerical calculations we have to represent the quantum states using available data structures. We construct sp states and use them to form antisymmetric Fock states. The creation and annihilation operators become functions that take the Fock states as arguments, and are used to create the Fock operators. Furthermore, the sum in the expression of the Fock operators can be optimized by only evaluating the non-zero terms.

5.4.1 Single-Particle-State Objects

We represent a single particle state with a record, i.e. an object with named fields that can be assigned values. It is natural to let each quantum number, such as l and j be a field. Moreover, we can include other information about the state, information that is taken for granted in the mathematical formulation. This includes a unique index for each state, the eigenvector holding information about the wavefunction, the basis of the eigenvector and, in the case of the plane wave basis, the contour used. Much of this extra information is redundant, as many states share the same information. Nevertheless, we found that this representation significantly simplifies the structure of the program and makes it easier to understand.

5.4.2 Fock State Objects and Operator Functions

An antisymmetric many-body state $|\alpha_1 \dots\rangle$ is represented by an ordered list of single particle objects and a sign. Since the sp state objects have a unique index, there is a well-defined sorting order. The sign can be 1, -1 or 0, representing $|\alpha_1 \dots\rangle$, $-|\alpha_1 \dots\rangle$ and 0, respectively.

The creation and annihilation operators are implemented as functions on the Fock state objects, obeying (5.10) to (5.15). The creation operator function steps through the list, flipping the sign at each step, until the correct place for the new particle is found. If the particle is already part of the Fock state, the sign is set to 0. The annihilation operator searches for a state, saves its index k in the list, annihilates it and set the sign to $(-1)^k$. If the state not exists, the sign is set to 0.

5.4.3 Fock Operator Matrix Elements

When computing matrix elements of a Fock space operator, most terms in the sum vanish. This is because most states will become zero when acted on by the creation and annihilation operators (equations (5.12) and (5.15)). Evaluating a sum of mostly zero elements is not very efficient, but this can be avoided by letting the sum run over just the single-particle states present in the bras and kets.

Chapter 6

The Nuclear Three-Body Problem

Equipped with the many-body theory of Chapter 5 we are now ready to study an open three-body system. The natural way to proceed is to add another neutron to our two-body ${}^5\text{He}$ system and form ${}^6\text{He}$, seen as an alpha particle core with two valence neutrons ($\alpha + n + n$). We now have to take into account the attractive two-body interaction between the neutrons, which allows for bound states in ${}^6\text{He}$ where there were none in ${}^5\text{He}$. Nuclei with this property are called *Borromean*, after the Borromean rings (Fig. 6.1). The Borromean rings are three rings interlocked in such a way that, if any one ring is removed, the other two will fall apart, as is the case with the core and the neutrons.

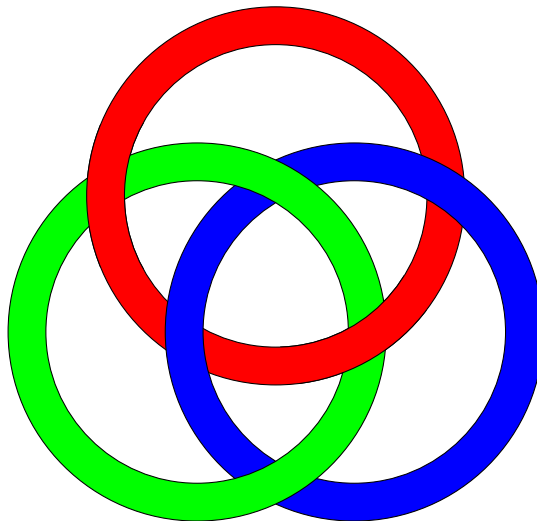


Figure 6.1: The Borromean rings

6.1 The ${}^6\text{He}$ Nucleus

We treat the ${}^6\text{He}$ system as a combination of two identical ${}^5\text{He}$ systems of core and neutron, i.e. two “one-particle” systems with the same reduced mass μ as in Chapter 3. The validity of this approach is not immediately obvious, but if the two neutrons have like parity there will be no recoil of the core [6]. The parity depends solely on l and we only consider neutrons in the p orbitals ($l = 1$), so the approach is valid.

The Hamiltonian takes on the form

$$\hat{H} = \hat{H}_1 + \hat{V}_{\text{res}} \quad (6.1)$$

where \hat{H}_1 is the Hamiltonian of the two-body problem and \hat{V}_{res} is the residual neutron-neutron interaction. To compute the Hamiltonian matrix we will use the eigensolutions $|E_i\rangle$ from the ${}^5\text{He}$ problem as single-particle basis states. We can do this because of the Berggren completeness relation (4.4), proving the completeness of this basis. Using the Berggren basis in this way to build more complex nuclei is referred to as the *Gamow Shell Model*.

The neutrons are fermions, so we form antisymmetric two-particle Fock states $|E_i, E_j\rangle$, according to the theory in Chapter 5. Because our basis consists of the eigenstates of \hat{H}_1 , we can use (5.19) and (5.25) to write the matrix elements as

$$\langle ab|\hat{H}|cd\rangle = \delta_{ac}\delta_{bd}(E_a + E_b) + \langle ab|V_{\text{res}}|cd\rangle, \quad (6.2)$$

where E_α are the energy eigenvalues of the two-body problem. Finally, the states are coupled according to Section 5.3 to reduce the size of the Hamiltonian matrix. The coupled matrix elements are

$$\langle ab; J|H|cd; J\rangle = \frac{1 + (-1)^J\delta_{ab}}{1 + \delta_{ab}}\delta_{ac}\delta_{bd}(E_a + E_b) + \langle ab; J|V_{\text{res}}|cd; J\rangle. \quad (6.3)$$

6.2 Neutron-Neutron Interaction

The interaction between nucleons is complex and there is no known analytical expression for the potential. It arises from the strong force between the quarks that make up the nucleons. The strong force is well known at high energies but less so at nuclear energy levels. The study of this interaction at the nuclear level is therefore an active field of research [7].

A convenient approximation is a *separable* interaction,

$$V(r_1, r_2) = v(r_1)v(r_2), \quad (6.4)$$

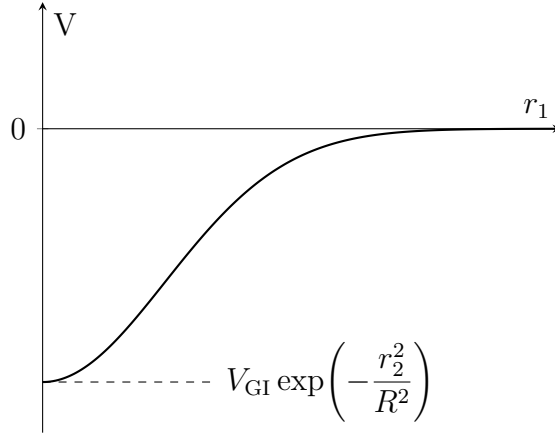


Figure 6.2: The Gaussian interaction potential as seen by one of the neutrons. The position of the other neutron determines the depth of the potential well.

a product of functions of r_1 and r_2 , the radii of each neutron. The interaction can be trivially separable as above or might require a *multipole expansion*, covered in [2]. We study two different types of separable two-body interactions, a gaussian interaction and a surface delta interaction.

6.2.1 Gaussian Interaction

Initially we investigate a trivially separable gaussian interaction

$$V(r_1, r_2) = -V_{\text{GI}} \exp\left(-\frac{r_1^2}{R^2}\right) \exp\left(-\frac{r_2^2}{R^2}\right). \quad (6.5)$$

The range R and strength V_{GI} are fitting parameters.

In Fig. 6.2 we see that the potential in a rough sense satisfies the expected properties of the interaction. If at least one neutron is far from the core, the other will experience little attraction. If both neutrons are in the vicinity of the core, they will experience a stronger attraction.

Because the potential is separable

$$V(r_1, r_2) = -V_{\text{GI}} V_{\text{sep}}(r_1) V_{\text{sep}}(r_2), \quad V_{\text{sep}}(r) = e^{-\frac{r^2}{R^2}} \quad (6.6)$$

we can write the two-body matrix elements as

$$(ab|V|cd) = -V_{\text{GI}} \langle a|V_{\text{sep}}|c\rangle \langle b|V_{\text{sep}}|d\rangle \quad (6.7)$$

which in the coupled scheme becomes

$$\begin{aligned} \langle ab; J|V|cd; J\rangle = & \\ & -V_{\text{GI}} \mathcal{N}_{ab} \mathcal{N}_{cd} \left(\langle a|V_{\text{sep}}|c\rangle \langle b|V_{\text{sep}}|d\rangle - (-1)^{j_1+j_2+J} \langle a|V_{\text{sep}}|d\rangle \langle b|V_{\text{sep}}|c\rangle \right). \end{aligned} \quad (6.8)$$

The $\langle a|V_{\text{sep}}(r)|c\rangle$ are calculated by expanding V_{sep} in the same basis as the sp states. In the momentum basis this is

$$\langle a|V_{\text{sep}}|c\rangle = \sum_i \sqrt{w_i} k_i \phi'_a(k_i) \sum_j \sqrt{w_j} k_j \phi'_b(k_j) V_{\text{sep}}(k_i, k_j), \quad (6.9)$$

with

$$V_{\text{sep}}(k_i, k_j) = \frac{2}{\pi} \int_0^\infty dr r^2 V(r) j_l(k_i r) j_l(k_j r), \quad (6.10)$$

as in Chapter 2

6.2.2 Surface Delta Interaction

Another possible interaction is the surface delta interaction (SDI)

$$V(\mathbf{r}_1, \mathbf{r}_2) = -V_{\text{SDI}} \delta(\mathbf{r}_1 - \mathbf{r}_2) \delta(r_2 - r_0) \quad (6.11)$$

where V_{SDI} is the strength and r_0 is the range, chosen to have the same value as the range of the Woods-Saxon potential.

The short-range strong force is thus approximated as a point interaction. The physical motivation of the $\delta(r - r_0)$ term is the experimental fact that the scattering cross-section between neutrons is inversely proportional to their kinetic energy. Since the kinetic energy has a minimum near the surface of the nucleus (at the range r_0 of the Woods-Saxon potential), we can approximate the interaction as focused entirely in that shell.

The SDI can be expanded into separable multipole radial components

$$v_l(r) = \frac{\delta(r - r_0)}{r}, \quad (6.12)$$

and with a complicated calculation (see [2]) one reaches the following expression for the coupled scheme matrix elements

$$\begin{aligned} \langle ab; J|V|cd; J\rangle &= -K_{abcd} \mathcal{N}_{ab}(J) \mathcal{N}_{cd}(J) (-1)^{l_a+l_c+j_b+j_d} \\ &\quad \times [1 + (-1)^{l_a+l_b+l_c+l_d}] [1 + (-1)^{l_c+l_d+J}] \\ &\quad \times \widehat{j}_a \widehat{j}_b \widehat{j}_c \widehat{j}_d \begin{pmatrix} j_a & j_b & J \\ \frac{1}{2} & -\frac{1}{2} & 0 \end{pmatrix} \begin{pmatrix} j_c & j_d & J \\ \frac{1}{2} & -\frac{1}{2} & 0 \end{pmatrix} \\ \mathcal{N}_{\alpha\beta} &= \frac{\sqrt{1 + (-1)^J \delta_{\alpha\beta}}}{1 + \delta_{\alpha\beta}} \\ K_{abcd} &= -\frac{V_0 r_0^2}{16\pi} \psi_a(r_0) \psi_b(r_0) \psi_c(r_0) \psi_d(r_0) \\ \widehat{j}_\alpha &= \sqrt{2j_\alpha + 1} \end{aligned} \quad (6.13)$$

$\psi_\alpha(r)$ being the radial wavefunction and the $\begin{pmatrix} j_1 & j_2 & j_3 \\ m_1 & m_2 & m_3 \end{pmatrix}$ are the Wigner 3j symbols.

6.3 The ${}^6\text{He}$ Solutions

We solve the ${}^6\text{He}$ Schrödinger equation in the coupled scheme, using (6.3) for the matrix elements. We first consider the Gaussian interaction, followed by the SDI. The parameters of our interactions are fitted to the known 0^+ ground state of ${}^6\text{He}$. Using the fitted parameters, we then make a prediction for the excited 2^+ state—a resonance. To find the resonance, we have to include the resonance of ${}^5\text{He}$ in the sp basis.

6.3.1 Identifying the Resonance

The solutions $|\psi\rangle$ will be written on the form

$$|\psi\rangle = \sum_{E_1 E_2} \Psi(E_1, E_2) |E_1 E_2; J\rangle \quad (6.14)$$

where the coefficients $\Psi(E_1, E_2)$ can be considered the wavefunction. These are not easily visualized because of the two variables, but they still can be used to obtain information about the solutions. Consider the component

$$\Psi(E_r, E_r) = \langle E_r^2; J | \psi \rangle, \quad (6.15)$$

being the overlap between a solution and the two-particle state corresponding to two independent ${}^5\text{He}$ resonances (here E_r denotes the energy of the ${}^5\text{He}$ $p_{3/2}$ resonance). It is found that the 2^+ resonance in ${}^6\text{He}$ predominantly consists of this component, allowing for an effective way to single out the relevant solution from a large set of scattering states.

6.3.2 Using the Gaussian Interaction

We begin by setting the range R of the gaussian potential to the same value as the Woods-Saxon range, 2 fm. The strength V_{GI} is fitted to reproduce the ${}^6\text{He}$ ground state. Because the Gaussian interaction is degenerate in J there is no distinction between the ground and excited states.

Decreasing the range to $R = 1$ fm, we find a wide resonance ($\Gamma > 6$ MeV), but this requires large values of k to be included in the basis and thus more scattering states. Although it might be possible to vary R and V_0 to get a resonance closer to experimental data, we do not pursue this method further.

6.3.3 Using the Surface Delta Interaction

The SDI has only one parameter, the strength V_{SDI} . However, because of its unphysical nature, it will also always depend on the truncation of the scattering states. We choose the smallest possible k_{max} for which the ${}^5\text{He}$ solutions converge, $k_{\text{max}} = 2.5 \text{ fm}^{-1}$. The strength is then fitted to the ground state of ${}^6\text{He}$ as before. The result is presented in Table 6.1.

Figure 6.3 shows all solutions $k = \sqrt{2\mu E}/\hbar$ obtained, plotted in the complex momentum plane. Most of the solutions correspond to energies on the form

$$E = E_1 + E_2 \quad \text{or} \quad k = \sqrt{k_1^2 + k_2^2} \quad (6.16)$$

where E_1 , E_2 , k_1 and k_2 are the energies of two ${}^5\text{He}$ eigenstates or their corresponding momenta. These solutions can be interpreted as two unbound particles, barely interacting with each other. This also explains the pattern that is seen—the momenta are all combinations of contour points that was used in the solution of ${}^5\text{He}$ to generate the basis.

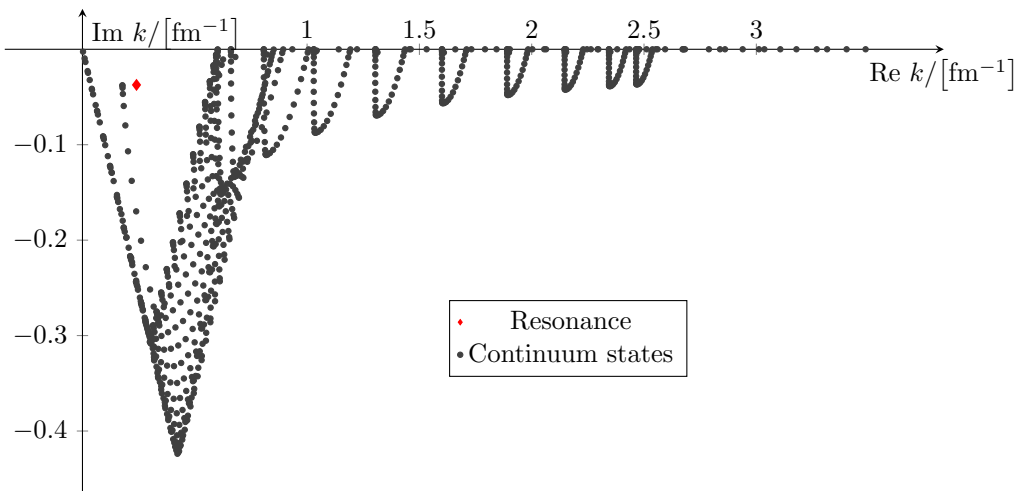


Figure 6.3: Momentum solutions for ${}^6\text{He}$, 2^+ . The resonance is located at $k = (0.241 - 0.037i) \text{ fm}^{-1}$. We have used the fitted Woods-Saxon parameters $V_0 = 47.05 \text{ MeV}$, $V_{\text{so}} = -7.04 \text{ MeV}$ and $k_{\text{max}} = 2.5 \text{ fm}^{-1}$. The SDI interaction was used with $V_0 = 998 \text{ MeV}$.

6.3.4 ${}^6\text{He}$ in the Real Momentum Basis

While it is required for the ${}^5\text{He}$ resonance to be included in the basis to find the excited 2^+ state, the ground state can be found without it. For a purely real contour, with all other parameters staying the same, a bound state with

Table 6.1: Experimental ${}^6\text{He}$ resonance data[4] and computed values with fitted Woods-Saxon parameters $V_0 = 47.05$ and $V_{\text{so}} = -7.04$. For the SDI, we used interaction strength $V_0 = 998$ MeV and range $r_0 = 2$. The Gaussian interaction used parameters $V_0 = 99$ MeV and $r_0 = 2$. 24 points were used on the contour for each basis. All values are in MeV.

J^π	Experiment	SDI	Gaussian
0^+	-0.975	-0.98	-0.97
2^+	0.8-0.55i	1.47-0.47i	-0.97

energy -0.976 MeV is found – almost identical to the result obtained with the Berggren basis.

Chapter 7

Outlook

We have studied resonances in Helium isotopes and given heuristic justifications for the methods used. The ${}^5\text{He}$ nucleus was modeled satisfactorily, and we could reproduce the experimental width and position of its resonances.

The Berggren basis obtained from the ${}^5\text{He}$ solutions was used to model the ${}^6\text{He}$ nucleus. The interactions used were simple first approximations, but while we were unable to reproduce the ${}^6\text{He}$ resonance with the gaussian interaction, the surface delta interaction gave us meaningful results. Consequently, an obvious way of improving upon our results is to use a more realistic potential. We have limited ourselves to a study of the energy spectrum, but one could also explore the ${}^6\text{He}$ system in more detail, e.g. looking at its density distribution [8].

Other areas to further explore, covered in more detail below, are: increasing the number of valence particles to study even more exotic systems, reducing the computational complexity through various techniques, combining the complex basis with other bases, better suited for describing bound states.

7.1 Realistic Two-Body Interactions

The phenomenological two-body interactions used in this thesis were chosen because of their simplicity, and there is much room for improvement. One approach is to make more educated guesses as to the form of the interaction, fitting parameters to experimental data for one system and trying to make predictions for other. Alternatively, one could begin from first principles by using knowledge of Quantum ChromoDynamics (QCD) and the strong interaction between the constituent quarks, the *ab initio* approach.

7.2 Additional Nucleons and Other Elements

We have studied the nuclei ${}^5\text{He}$ and ${}^6\text{He}$ in a few-body picture as a two- and three-body problem consisting of a core and one or two valence particles respectively. A natural extension is to stay in the same picture, adding more neutrons to study the more exotic ${}^7\text{He}$ and ${}^8\text{He}$. With more particles has to consider the angular momentum coupling of three or four particles. Other than that the techniques we employ are general.

Another possibility is to study other elements than helium, still in the core with valence neutron model. ${}^{16}\text{O}$ and ${}^{24}\text{O}$ are good candidates, since they too are doubly magic nuclei. Other light elements like Li or Be are of interest as well, as they like He, display several interesting properties of open quantum systems. One has to take into consideration that they do not have a well-defined core though. This could make them suitable subjects for the methods described here.

When expanding ${}^6\text{He}$, our basis consists of only $p_{1/2}$ and $p_{3/2}$ waves. This is a good approximation for ${}^6\text{He}$ [3], but for other systems, more partial waves may be needed. This poses additional challenges, since one needs to introduce a transitionally invariant coordinate systems when treating particles of mixed parity.

7.3 Reducing Computation Time

With an increased number of particles, the size of the Hamiltonian matrix grows exponentially. This leads to more matrix element calculations, memory usage requirements and slower diagonalization.

One way to reduce the matrix size is to select only the most important basis states in computations. This is possible because certain many-body configurations barely give any contribution to the energy of the (quasi-)bound solutions. An example of a method doing this is the Density Matrix Renormalization Group (DMRG) [9].

Another, less systematic, approach is the Monte Carlo method of randomly sampling states to include and taking the mean. We made a minor study of a potential Monte-Carlo approach, but cannot present any conclusive results. We want to encourage further research on this topic, though, as the method, while simple, could prove a useful tool.

While a larger system requires more matrix elements, many of the elements are zero. As the size of the matrix grows, it is eventually no longer efficient to store them as an array. Instead, a *sparse-matrix* representation is employed, which only stores information about the non-zero elements.

Furthermore, while working with sparse matrices one has to adapt the diagonalization (eigensolver) algorithms. The Lanczos algorithm is the most commonly used method for large, sparse matrices. It generally extracts the largest or smallest eigenvalues, but resonances can exist in the middle of the spectrum, so some adaptations might be required. It is also important to note that our complex-momentum approach gives us a non-hermitian symmetric matrix while most eigensolvers expect matrices to be hermitian. A possible development is then to research eigensolver for non-hermitian (but symmetric) matrices.

Bibliography

- [1] T. Berggren, “On the use of resonant states in eigenfunction expansions of scattering and reaction amplitudes,” *Nuclear Physics A*, vol. 109, pp. 265–287, 1968.
- [2] J. Suhonen, *From Nucleons to Nucleus*. Springer, 2007.
- [3] N. Michel, W. Nazarewicz, M. Płoszajczak, and K. Bennaceur, “Gamow Shell Model Description of Neutron-Rich Nuclei,” *Physical Review Letters*, vol. 89, p. 042502, July 2002.
- [4] D. Tilley, C. Cheves, J. Godwin, G. Hale, H. Hofmann, J. Kelley, C. Sheu, and H. Weller, “Energy levels of light nuclei $a=5, 6, 7$,” *Nuclear Physics A*, vol. 708, no. 1–2, pp. 3 – 163, 2002.
- [5] W. H. Dickhoff and D. V. Neck, *Many-Body Theory Exposed!* World Scientific Publishing, 2005.
- [6] Y. Suzuki and K. Ikeda, “Cluster-orbital shell model and its application to the He isotopes,” *Physical Review C*, vol. 38, pp. 410–413, July 1988.
- [7] C. Forssén, G. Hagen, M. Hjorth-Jensen, W. Nazarewicz, and J. Rotureau, “Living on the edge of stability, the limits of the nuclear landscape,” *Physica Scripta Volume T*, vol. 152, p. 014022, Jan. 2013.
- [8] G. Papadimitriou, A. T. Kruppa, N. Michel, W. Nazarewicz, M. Płoszajczak, and J. Rotureau, “Charge radii and neutron correlations in helium halo nuclei,” , vol. 84, p. 051304, Nov. 2011.
- [9] J. Rotureau, N. Michel, W. Nazarewicz, M. Płoszajczak, and J. Dukelsky, “Density Matrix Renormalization Group Approach for Many-Body Open Quantum Systems,” *Physical Review Letters*, vol. 97, p. 110603, Sept. 2006.
- [10] M. Moshinsky and Y. F. Smirnov, *The Harmonic Oscillator in Modern Physics*. Harwood Academic Publishers, 1996.

- [11] R. Mehrem, “The plane wave expansion, infinite integrals and identities involving spherical bessel functions,” *Applied Mathematics and Computation*, vol. 217, pp. 5360–5365, 2011.
- [12] G. H. Golub and J. H. Welsch, “Calculation of gauss quadrature rules,” *Mathematics of Computation*, vol. 23, no. 106, pp. pp. 221–230+s1–s10, 1969.
- [13] M. Abramowitz and I. A. Stegun, *Handbook of Mathematical Functions with Formulas, Graphs, and Mathematical Tables*. New York: Dover, ninth dover printing, tenth gpo printing ed., 1964.

Appendix A

Derivations

A.1 Harmonic Oscillator Matrix Elements

First, we express the Hamiltonian H of our problem in terms of H_{HO} (2.12) to get

$$H = H_{\text{HO}} - \frac{\mu\omega^2 r^2}{2} + V(r). \quad (\text{A.1})$$

We then close this equation with $\langle nlm|$ on the left and $|n'lm\rangle$ on the right to get three terms on the RHS, which we consider in turn. The first is just the eigenvalues of H_{HO}

$$\langle nlm|H_{\text{HO}}|n'lm\rangle = E_{nl}\langle nlm|n'lm\rangle = \hbar\omega\left(2n + l + \frac{3}{2}\right)\delta_{nn'}. \quad (\text{A.2})$$

The second follows from the known identity [10]

$$\begin{aligned} \langle nlm|r^2|n'lm\rangle = \\ \frac{\hbar}{\mu\omega} \left(\left(2n + l + \frac{3}{2}\right)\delta_{nn'} - \sqrt{n(n+l+\frac{1}{2})}\delta_{n,n'-1} - \sqrt{n'(n'+l+\frac{1}{2})}\delta_{n',n-1} \right). \end{aligned} \quad (\text{A.3})$$

The third term is calculated in the position basis, with

$$\langle \mathbf{r}|nlm\rangle = R_{nl}(r)Y_l^m(\theta, \phi), \quad (\text{A.4})$$

where R_{nl} is the HO radial wavefunctions (see (2.16)) and Y_l^m are the spherical harmonics. Because $V(r)$ is spherically symmetric, the spherical harmonics integrate to 1 and we get

$$\langle nlm|V(r)|n'lm\rangle = \int_0^\infty dr r^2 R_{nl}(r)V(r)R_{n'l}(r). \quad (\text{A.5})$$

Putting it all together, we have

$$\begin{aligned}
\langle nlm|H|n'lm\rangle &= \langle nlm|H_{\text{HO}} - \frac{\mu\omega^2 r^2}{2} + V(r)|n'lm\rangle \\
&= \frac{\hbar\omega}{2} \left(\left(2n + l + \frac{3}{2}\right) \delta_{nn'} + \sqrt{n(n+l+\frac{1}{2})} \delta_{n,n'-1} \right. \\
&\quad \left. + \sqrt{n'(n'+l+\frac{1}{2})} \delta_{n',n-1} \right) + \int_0^\infty dr r^2 R_{nl}(r) V(r) R_{n'l}(r).
\end{aligned} \tag{A.6}$$

A.2 Radial Momentum Space TISE

To find the momentum space Schrödinger equation, we need to write an explicit expression for

$$\int d^3\mathbf{k}' \langle \mathbf{k}|H|\mathbf{k}'\rangle \Phi(\mathbf{k}') = E\Phi(\mathbf{k}) \tag{A.7}$$

To begin with, using the completeness relation with the position basis, we note that

$$\Phi(\mathbf{k}) = \langle \mathbf{k}|\psi\rangle = \int d^3\mathbf{r} \langle \mathbf{k}|\mathbf{r}\rangle \psi(\mathbf{r}) \tag{A.8}$$

Standard textbooks on quantum mechanics show

$$\langle \mathbf{k}|\mathbf{r}\rangle = \frac{1}{(2\pi)^{\frac{3}{2}}} e^{i\mathbf{k}\cdot\mathbf{r}}. \tag{A.9}$$

For a spherically symmetric problem, solutions can be found on the form $\psi(\mathbf{r}) = R(r)Y_l^m(\Omega_r)$. We can simplify the above integral by using the plane wave expansion [11]

$$e^{i\mathbf{k}\cdot\mathbf{r}} = 4\pi \sum_{l=0}^{\infty} \sum_{m=-l}^l i^l j_l(kr) Y_l^m(\Omega_k) Y_l^m(\Omega_r)^* \tag{A.10}$$

where you can choose either factor to conjugate.

Inserting this and using orthogonality of spherical harmonics

$$\int d\Omega_r Y_l^{m'*}(\Omega_r) Y_l^m(\Omega_r) = \delta_{mm'} \delta_{ll'} \tag{A.11}$$

you obtain

$$\Phi(\mathbf{k}) = \phi(k) Y_l^m(\Omega_k) = \sqrt{\frac{2}{\pi}} i^l Y_l^m(\Omega_k) \int dr r^2 R(r) j_l(kr). \tag{A.12}$$

In a similar manner, we evaluate

$$\begin{aligned}
\langle \mathbf{k} | V(r) | \mathbf{k}' \rangle &= \frac{1}{(2\pi)^3} \int d^3 \mathbf{r} V(r) e^{i\mathbf{k}' \cdot \mathbf{r}} e^{-i\mathbf{k} \cdot \mathbf{r}} \\
&= \frac{1}{(2\pi)^3} (4\pi)^2 \sum_{l, l'} \sum_{m, m'} (-1)^l i^{l+l'} Y_{l'}^{m'*}(\Omega_{k'}) Y_l^m(\Omega_k) \\
&\quad \times \int dr r^2 V(r) j_l(kr) j_{l'}(k'r) \int d\Omega_r Y_{l'}^{m'}(\Omega_r) Y_l^{m*}(\Omega_r)
\end{aligned} \tag{A.13}$$

Here, a factor $(-1)^l$ was introduced because of the parity of the spherical harmonics: $Y_l^m(-\Omega_k) = (-1)^l Y_l^m(\Omega_k)$.

Inserting all of this into the Schrödinger equation and again simplifying by using the orthogonality of the spherical harmonics twice, you immediatly obtain the sought after equation

$$\begin{aligned}
\int d^3 \mathbf{k}' \langle \mathbf{k} | H | \mathbf{k}' \rangle \Phi(\mathbf{k}') &= \frac{k^2}{2\mu} \phi(k) Y_l^m(\Omega_k) + \int_{\mathbb{R}^3} d^3 \mathbf{k}' \langle \mathbf{k} | V(r) | \mathbf{k}' \rangle \phi(k') Y_l^m(\Omega_{k'}) \\
&= \frac{k^2}{2\mu} \phi(k) Y_l^m(\Omega_k) + Y_l^m(\Omega_k) \int_0^\infty dk' k'^2 \phi(k') V(k, k') \\
&= E \phi(k) Y_l^m(\Omega_k)
\end{aligned} \tag{A.14}$$

where

$$V(k, k') = \frac{2}{\pi} \int dr r^2 V(r) j_l(kr) j_l(k'r). \tag{A.15}$$

Appendix B

Numerical Integration

B.1 Gauss-Legendre Quadrature

One notices that conventional integrals are computationally taxing. A conventional integral approximation is to evaluate the function in evenly spaced points with a weighted by the step length. This, however requires many points to converge and quickly becomes unwieldy in computations.

That is why one should use the Gauss-Legendre quadrature; through a clever choice of points and weights the integral will converge with fewer points. The theory behind this approximation is involved [12] and is not covered here.

The idea is to pick points x_i on the $[-1, 1]$ interval that are roots of the Legendre polynomial of a certain degree n and approximate the integral with

$$\int_{-1}^1 f(x) dx \approx \sum_{i=1}^n w_i f(x_i). \quad (\text{B.1})$$

with the weights given by [13]

$$w_i = \frac{2}{(1 - x_i^2)[P'_n(x_i)]^2} \quad (\text{B.2})$$

where P_n is the Legendre polynomial of degree n . This can be rescaled for any definite integral

$$\int_a^b f(x) dx \approx \frac{b-a}{2} \sum_{i=1}^n w_i f\left(\frac{b-a}{2}x_i + \frac{a+b}{2}\right). \quad (\text{B.3})$$

It can be shown that this quadrature gives the correct value for all polynomials of degree up to $2n - 1$. The only requirement for convergence is that the integrand can be approximated by a polynomial on the interval. In some cases, as with singular functions, that is not possible, but for the functions encountered in this work it is a safe approximation.

Appendix C

Tools

All the computations were implemented in the Python programming language using the libraries NumPy and SciPy. We used the TikZ and pgfplots libraries to make the figures. The code was managed using Git and is available at

<https://github.com/pnutus/NHQM>